Electromagnetic inverse problems for nematic liquid crystals and capacitance imaging

Polydorides, Nick

2004

MIMS EPrint: **2007.15**

Manchester Institute for Mathematical Sciences
School of Mathematics

The University of Manchester

Reports available from: http://eprints.maths.manchester.ac.uk/
And by contacting: The MIMS Secretary
School of Mathematics
The University of Manchester
Manchester, M13 9PL, UK

ISSN 1749-9097

ELECTROMAGNETIC INVERSE PROBLEMS FOR NEMATIC LIQUID CRYSTALS AND CAPACITANCE IMAGING.

NICK POLYDORIDES

Abstract. The aim of this study is to formulate and solve the high-frequency electromagnetic problem of wave propagation through nematic liquid crystal cells of arbitrary shape, and subsequently approach the inverse problem of reconstructing the orientational order by means of recovering the dielectric tensors in the interior from a finite set of boundary polarization measurements. The numerical solution of the forward electromagnetic problem is achieved by hybridizing the conventional vector finite elements with a boundary integral method, so that to preserve the necessary continuity conditions for the electromagnetic fields at the boundary of the domain. Combining the finite element equations with a magnetic field integral boundary equation yields surface integrals involving Green's function and its gradient. These integrals have kernels that become asymptotically singular as the distance between the observation and integration points reduces to zero, essentially making the numerical integration process problematic. For their computation a new basis of functions are introduced for the surface current density, the so-called Rao-Wilton-Glisson functions, which effectively substitute the tangential components of the magnetic field in the original boundary integrals. The transformed integrals are then treated with the singularity extraction method, essentially separating the smooth from the singular components of the kernels, the former of which are computed using conventional numerical integration and the later using closed form expressions derived for the RWG functions. The forward problem is then linearized with the aid of the Fréchet derivative of the forward Maxwell operator and subsequently regularized using a Tikhonov type regularization. In regularization we construct a penalty term based on Frank's distortion energy functional, which is known to have a minimum in the neighborhood of stable liquid crystal director configurations. The inverse problem of reconstructing the orientation of the director vector in a uniaxial nematic liquid crystal using a finite set of noise infused boundary polarization measurements is approached as a special case of the inverse permittivity tensor problem, where the dielectric tensors are symmetric and expected to vary most significantly along the directions of their two biggest eigenvalues, which correspond to the associated Euler angles of the director vector.

1. Introduction

Grating aligned nematic liquid crystals (NLC) are of interest to the researchers and manufacturers of displays and other optical devices. In order to understand and optimize these devices one needs to be able to probe the liquid crystal director orientation profile around and beyond the grating structure. According to

Received by the editors November 2004 and, in revised form, January 6 2005.

Key words and phrases. Nematic liquid crystals, vector finite elements, finite element boundary integral method, director orientation, singular integrals.

The author is grateful to the Smith Institute for the Faraday Partnership, EPSRC for the grant GR/R93612/01 and Hewlett Packard Laboratories Bristol for their support.

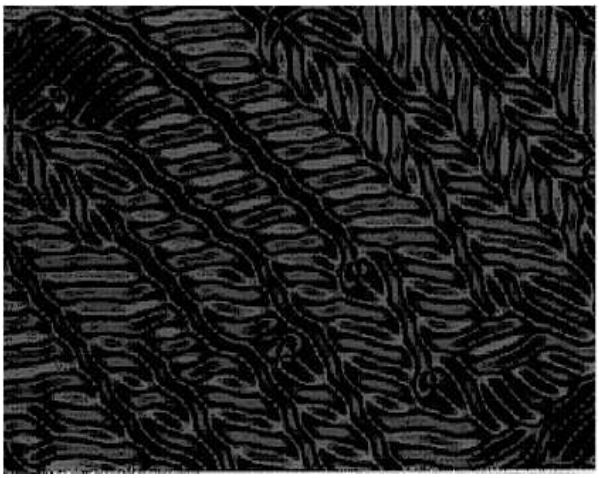

FIGURE 1. Image of a biaxial nematic liquid crystal cell as obtained for a polarized microscope. On the image note the distinctive oval shape of the molecules and the nonuniform profile of the director.

a recent report by Newton et al. [25], in the design of liquid crystal displays, the optimum goal for displays is to maximize the contrast and achieve at least a 300 dpi resolution. To achieve this, researchers have resorted in numerical models that allow them to obtain an understanding on how the light propagates inside the liquid crystal. In this context, monitoring how the polarization state of the laser changes as it propagates along the liquid crystal cell, can yield information about the orientational order of its molecular structure. For the bistable NLC in particular the aim is to generate a model which is accurate enough to track the various stable states and also efficient enough to be implemented for laboratory research using realistic design space. This hints to the need for considering the inverse problem of recovering the interior electro-optical properties of the devices from acquired boundary observations. The high-frequency liquid crystal problem is closely related to other electromagnetic problems at lower frequencies, in particular the use of low-frequency electrostatic and electromagnetic measurements for location, detection and imaging problems [28].

The aim of this work is to solve the ill-posed inverse electromagnetic (EM) problem of determining the profile of the orientation of the director vector in a uniaxial NLC using a finite set of noise infused optical measurements. This will be treated as a special high-frequency case of the inverse permittivity tensor reconstruction problem in Maxwell's time-harmonic equations. Parts of the derived methodology will subsequently extended to cover the low-frequency electrical capacitance imaging problem, seeking to recover the distribution of permittivity tensors in the half space from boundary current intensity measurements. A complete suite of MATLAB [23] routines for solving the forward and ill-posed inverse anisotropic permittivity problems on finite domains, will be designed as part of this research.

1.1. **Existing technology.** In their technical report [25], the authors follow an electro-optical strategy in deriving a model that enables the recovery of the director configuration within the cell by minimizing the free energy stored inside the liquid crystal. This approach preserves the stability of the reconstructed solution as well as its compliance with Maxwell's equations. The total energy is known to be the sum of the elastic distortion energy density, the surface energy density, the dielectric energy density and the flexoelectric energy density, all of which can be expressed in terms of the director and its spatial derivatives. For more details see the textbooks by Chandrasekhar [5] and de Gennes et al. [11]. The authors make use of the Berreman 4×4 matrix approach for wave propagation in layered media [2], and some of its computationally efficient variants like the extended 2×2 Jones matrix method [10], often providing sufficient accuracy for many one-dimensional problems. In these, a medium consisted of a finite sequence of homogenous anisotropic layers is considered, with the layers aligned perpendicularly on the z axis while extending to infinity in x and y axes, and the permittivity tensors are taken to vary periodically only along the direction of the propagation. In Berreman's model, the six components of the electromagnetic radiation $\mathbf{E}_i$ and $\mathbf{H}_i$ for $i = x, y, z$ are effectively reduced to four, the so called Berreman vector, by expressing the components of the electromagnetic fields along the axis of propagation (longitudinal components) in terms of the transverse. For incident monochromatic plane waves of arbitrary polarization, impinging the model obliquely in its origin, e.g. the $z = 0$ plane, the component of propagation along the x direction is taken constant, while that along the y direction vanishes. In essence, these assumptions cause Maxwell's equations to reduce to the linear ordinary differential equation

$$\frac{d\psi^b}{dz} = -jk_0 \Delta \psi^b \tag{1.1.1}$$

where $k_0 = 2\pi/\lambda$, Δ is the 4×4 Berreman matrix and $\psi^b = \begin{bmatrix} \mathbf{E}_x & \mathbf{H}_y & \mathbf{E}_y & -\mathbf{H}_x \end{bmatrix}^T$ is the Berreman vector. This vector will appear also in our numerical model to be described further on.

While these analytic methods offer acceptable results in some simple NLC configurations [41], in general these are inadequately equipped to handle realistic models of arbitrary boundary shape, e.g. gratings, and permittivity distributions that vary in all spatial dimensions. In two and three dimensional problems involving cells whose lateral dimensions are comparable to their thickness, a number of stable director configurations are possible for a given geometry and electrical driving conditions, making the modelling more complicated. Overall, the modelling complexity increases considerably when the third dimension is considered, but at the same time the shortcomings of the one-dimensional modelling strategies are exposed. The geometry of the problem must be defined in the three-dimensional Cartesian space in a way to incorporate possible deformations and distortions in the orientation of the liquid crystal layers along with any local defects and the respective boundary conditions. In particular, liquid crystals with gratings present a number of practical difficulties for the Berreman model, and therefore the use of numerical approximation technique such as the vector finite element method is more appropriate in this respect.

Consider a monochromatic plane wave of arbitrary polarization p_{in} driven acutely into a NLC cell at the incidence part of the boundary, then propagating through the liquid crystal and subsequently emerging out of the cell and through a collinear

polarimeter which records a polarization p_{out}. This experiment is repeated for a number of input polarization settings and incidence angles until enough data is gathered. In this case, the objective of the corresponding inverse problem is to reconstruct images of the profile of the director vector $\mathbf{x}$ in its interior from measurements of polarization perturbations $p_{in} - p_{out}$. The problem is regarded as a special case of the generic permittivity reconstruction problem, since the dielectric tensor within the nematic liquid crystal is known to vary more significantly along the direction of its two most distinguished eigenvalues, say λ_1 and λ_2, which in fact are directly related to the two Euler angles of the unitary director vector 2. In response our aim is to recover dielectric tensors of the form

$$\boldsymbol{\epsilon} = (\lambda_1 - \lambda_2)\,\mathbf{x} \otimes \mathbf{x} + \lambda_2\, I \tag{1.1.2}$$

where $\mathbf{x} \in \mathbb{R}^3$, $\|\mathbf{x}\|_2 = 1$ is the director and I is the 3×3 identity matrix. Nematic liquid crystals can be described on the continuum level by a director field $\mathbf{x}(\mathbf{r})$ which is the average direction of a small sample of molecules around the point $\mathbf{r}$. Since $\mathbf{x}$ represents only a direction, the modulus is fixed, $\mathbf{x}^2 = 1$. The inversion of a nematic molecule does not change its physical properties. This fact is reflected in the further symmetry requirement $\mathbf{x} = -\mathbf{x}$, which makes nematics different from a simple vector-field system [30]. From the elasticity theory stable director configurations in nematics with no interior defects minimize the bulk distortion energy functional (Kriezis et al. [20])

$$\arg\min_{\mathbf{x}} \int_{\Omega} (F_\nu + F_s)\, \mathrm{d}\Omega \tag{1.1.3}$$

where

$$F_\nu = \frac{1}{2}\Big(K_{11}(\nabla \cdot \mathbf{x})^2 + K_{22}(\mathbf{x} \cdot \nabla \times \mathbf{x})^2 + K_{33}\big(\mathbf{x} \times (\nabla \times \mathbf{x})\big)^2\Big) \tag{1.1.4a}$$

and

$$F_s = \frac{1}{2}\Big(\frac{K_{11}}{a_1}(\mathbf{x} \cdot \hat{\mathbf{n}}_{s1})^2\delta(p_1) + \frac{K_{11}}{a_2}(\mathbf{x} \cdot \hat{\mathbf{n}}_{s2})^2\delta(p_2)\Big) \tag{1.1.4b}$$

In the equations above a_1, a_2 are the anchoring extrapolation areas on the surfaces upon which the light enters and leaves the liquid crystal, $\hat{\mathbf{n}}_{s1}, \hat{\mathbf{n}}_{s2}$ are the outward unit normals on these surfaces and $\delta(p1), \delta(p2)$ are delta functions restraining the energy within the liquid crystal. The presence of topological defects with their core surfaces tangible on the boundary of the cell makes the surface term F_s problematic to compute, thus for the needs of of this study we assume $F_s \sim 0$.

In uniaxial dielectrics the dielectric tensor is described by an axis parallel to the director ($\mathbf{x}_\parallel$), and a degenerate axis lying in any direction perpendicular to the plane of the director ($\mathbf{x}_\perp$), while for the biaxial dielectrics, the permittivity tensor is specified with the aid of the three principal axes, $\mathbf{x}_1 \neq \mathbf{x}_2 \neq \mathbf{x}_3$, like

$$\boldsymbol{\epsilon}^{uniaxial} = \begin{bmatrix} \mathbf{x}_\perp & 0 & 0 \\ 0 & \mathbf{x}_\perp & 0 \\ 0 & 0 & \mathbf{x}_\parallel \end{bmatrix} \quad \text{and} \quad \boldsymbol{\epsilon}^{biaxial} = \begin{bmatrix} \mathbf{x}_1 & 0 & 0 \\ 0 & \mathbf{x}_2 & 0 \\ 0 & 0 & \mathbf{x}_3 \end{bmatrix} \tag{1.1.5}$$

From the Q tensor theory as in [24] and [11], the director of the uniaxial nematic can be parameterized in terms of the two azimuthal Euler angles as

$$\mathbf{x}(\theta, \phi) = \begin{bmatrix} \cos\theta\, \cos\phi & \cos\theta\, \sin\phi & \sin\theta \end{bmatrix} \tag{1.1.6}$$

The angles are those appearing in the schematic of figure 2. Using the scalar

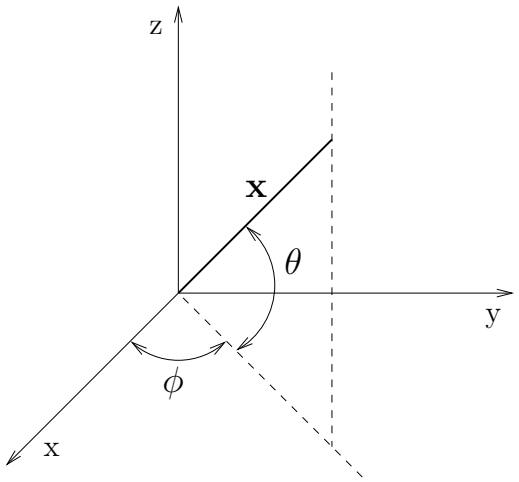

FIGURE 2. The director $\mathbf{x}$ in terms of the Euler angles θ and ϕ.

order parameter S, which is a measure of how much the main axes of the nematic molecules deviate from the director, and the two Euler angles we can write a 3×3 matrix $\mathbf{M} = S(\mathbf{x} \otimes \mathbf{x})$ that describes the nematic state. More conventionally though, instead of $\mathbf{M}$ one forms the $\mathbf{Q}$ tensor

$$\mathbf{Q} = S\,(\mathbf{x} \otimes \mathbf{x}) - \frac{1}{3} S\,I \tag{1.1.7}$$

The entries of the symmetric traceless $\mathbf{Q}$ are given by

$$\begin{bmatrix} q_1 & q_2 & q_3 \\ q_2 & q_4 & q_5 \\ q_3 & q_5 & -q_1 - q_4 \end{bmatrix}$$

where $q_1 = S\cos^2\theta\cos^2\phi - 1/3\,S$, $q_2 = S\cos^2\theta\sin\phi\cos\phi$, $q_3 = S\sin\theta\cos\theta\cos\phi$, $q_4 = S\cos^2\theta\sin^2\phi - 1/3\,S$, and $q_5 = S\cos\theta\sin\theta\sin\phi$, while in a uniaxial nematic diagonalizing $\mathbf{Q}$ yields a matrix with three eigenvalues (entries)of multiplicity one and two, $\lambda_1 = 2/3\,S$, and $\lambda_{2,3} = -1/3\,S$, therefore in agreement with the expression in (1.1.5).

This study refers primarily in the recovery of the director vector in a uniaxial nematic liquid crystal cell, in which case the molecules are oriented on the average along the director. However, the presence of thermal fluctuations or confining surfaces impairs this ideal configuration, causing a local distortion of the orientational. This distortion, a perturbation in director orientation, has a profound impact on Frank's energy functional (1.1.3) and can be traced and localized by formulating the appropriate inverse problem director problem. In order to derive the inverse problem one has to formulate and solve the forward problem of wave propagation within the nematic cell. The starting point for this is Maxwell's time-harmonic equations which is discussed in some detail next.

2. Maxwell's equations

The mathematical framework for electromagnetics is derived from Maxwell's equations. In a closed domain Ω, where the material properties behave linearly

with respect to the applied electromagnetic fields, Maxwell's equations are given by

$$\begin{aligned} \nabla\times\mathbf{E}(\mathbf{r},t) &= -\frac{\partial\mathbf{B}(\mathbf{r},t)}{\partial t} + \mathbf{J}(\mathbf{r},t) \\ \nabla\times\mathbf{H}(\mathbf{r},t) &= \frac{\partial\mathbf{D}(\mathbf{r},t)}{\partial t} - \mathbf{M}(\mathbf{r},t) \\ \nabla\cdot\mathbf{D}(\mathbf{r},t) &= 0 \\ \nabla\cdot\mathbf{B}(\mathbf{r},t) &= 0 \end{aligned} \tag{2.0.8}$$

where $\mathbf{E}$ is the electric field in [V/m], $\mathbf{H}$ is the magnetic field in [A/m], $\mathbf{J}$ is the electric current density in [A/m^2], $\mathbf{M}$ is the magnetic current density in [V/m^2], while $\mathbf{D}$ and $\mathbf{B}$ are the electric and magnetic flux density fields in [C/m^2] and [Wb/m^2] respectively. Moreover, the constructive relations

$$\begin{aligned} \mathbf{D}(\mathbf{r},t) &= \epsilon(\mathbf{r})\mathbf{E}(\mathbf{r},t) \\ \mathbf{B}(\mathbf{r},t) &= \mu(\mathbf{r})\mathbf{H}(\mathbf{r},t) \end{aligned} \tag{2.0.9}$$

hold, where ϵ is the electrical permittivity in [F/m] and μ the magnetic permeability in [H/m]. In media with isotropic electrical properties, that is where ϵ and μ are scalar fields, $\mathbf{E}$ and $\mathbf{D}$ differ only in magnitude, while the same holds for the magnetic field and its flux density. In anisotropic media on the other hand, where ϵ and μ are tensor fields, this resemblance is no longer valid, in that EM field intensities and fluxes are vector fields that point in different directions. The total current density in the domain is evaluated as the sum of the impressed electric and magnetic sources in the interior or the boundary of the domain and the induced currents as

$$\begin{aligned} \mathbf{J} &= \mathbf{J}_i + \sigma\mathbf{E} \\ \mathbf{M} &= \mathbf{M}_i + \sigma_m\mathbf{H} \end{aligned} \tag{2.0.10}$$

where $\mathbf{J}_i$, $\mathbf{M}_i$ are the i'th electric and magnetic current sources respectively, σ is the electrical conductivity of the domain in [S/m] and σ_m is the magnetic current conductivity in [Ω/m]. The space-frequency formulation of Maxwell's time harmonic equations can be derived by assuming a time dependence of $\exp(-j\omega t)$ in the set of equations (2.0.8), where $\omega = 2\pi f$ is the angular frequency of the signals in [Hz], and $j = \sqrt{-1}$. In effect, the electromagnetic fields inside Ω satisfy

$$\begin{aligned} \nabla\times\mathbf{H}(\mathbf{r},\omega) - \big(\sigma(\mathbf{r}) + j\omega\epsilon(\mathbf{r})\big)\,\mathbf{E}(\mathbf{r},\omega) &= \mathbf{J}(\mathbf{r},\omega) \\ \nabla\times\mathbf{E}(\mathbf{r},\omega) + j\omega\mu(\mathbf{r})\,\mathbf{H}(\mathbf{r},\omega) &= -\mathbf{M}(\mathbf{r},\omega) \\ \nabla\cdot\mathbf{D}(\mathbf{r},\omega) &= 0 \\ \nabla\cdot\mathbf{B}(\mathbf{r},\omega) &= 0 \end{aligned} \tag{2.0.11}$$

In the remaining text, the frequency dependence and the position vector of the fields are suppressed when implied to improve clarity in the notation. Substituting the magnetic field from the first equation into the second and solving for the electric field yields

$$-\nabla\times\Big(\frac{1}{\mu}\nabla\times\mathbf{E}\Big) + \Big(\omega^2\epsilon - j\omega\sigma\Big)\mathbf{E} = j\omega\,\mathbf{J} + \nabla\times\frac{1}{\mu}\,\mathbf{M}$$

Multiplying with $(-\mu_0)$, we arrive at the electric field dependent equation

$$\nabla \times \Big(\frac{1}{\mu_r}\nabla \times \mathbf{E}\Big) + \Big(jk_0 Z_0 \sigma - k_0^2 \epsilon_r\Big)\mathbf{E} = -jk_0 Z_0\, \mathbf{J} - \nabla \times \frac{1}{\mu_r}\mathbf{M} \tag{2.0.12}$$

Similarly, substituting and solving for the magnetic field leads to the dual of (2.0.12)

$$\nabla \times \Big(\frac{1}{\epsilon_r}\nabla \times \mathbf{H}\Big) + \Big(jk_0 Y_0 \sigma - k_0^2 \mu_r\Big)\mathbf{H} = -jk_0 Y_0\, \mathbf{M} - \nabla \times \frac{1}{\epsilon_r}\,\mathbf{J} \tag{2.0.13}$$

where $\epsilon = \epsilon_0\epsilon_r$, $\mu = \mu_0\mu_r$, $k_0 = 2\pi\lambda_0^{-1} = \omega\sqrt{\epsilon_0\mu_0}$, $Z_0 = \sqrt{\mu_0\epsilon_0^{-1}}$ and $Y_0 = Z_0^{-1}$ In the above relations, $\epsilon_0 = 8.854 \times 10^{12}$ is the free-space permittivity number in [F/m], $\mu_0 = 4\pi \times 10^{-7}$ is the free-space permeability number in [H/m], k_0 is the free-space wave number in [1/m] and λ_0 is the free-space wavelength in [m], Z_0 is the free-space impedance in [Ω] and Y_0 the corresponding admittance in [S]. Using the vector identity

$$\nabla \times (u\mathbf{A}) = \nabla u \times \mathbf{A} + u\nabla \times \mathbf{A}$$

equation (2.0.12) can be written as

$$\mu_r^{-1}\nabla \times \nabla \times \mathbf{E} - k_0^2\epsilon_r\mathbf{E} + \Big[\nabla\mu_r^{-1} \times \nabla \times \mathbf{E}\Big] = -jk_0 Z_0\mathbf{J} - \nabla \times \mu_r^{-1}\mathbf{M} \tag{2.0.14}$$

In a homogeneous, source and charge free medium of $\epsilon_r = \mu_r = 1$, $\nabla\mu_r^{-1} = 0$, $\mathbf{J} = \mathbf{M} = 0$ and $\nabla \cdot \epsilon\mathbf{D} = 0$, hence the above equation simplifies to

$$\nabla \times \nabla \times \mathbf{E} - k_0^2\mathbf{E} = 0 \tag{2.0.15}$$

and using the property

$$\nabla \times \nabla \times \mathbf{A} = \nabla(\nabla \cdot \mathbf{A}) - \nabla^2\mathbf{A}$$

we arrive at the familiar form of the *scalar wave* Helmholtz equation

$$\nabla^2 u - k_0^2 u = 0 \tag{2.0.16}$$

satisfied for each $u = \mathbf{E}^{(x)}, \mathbf{E}^{(y)}, \mathbf{E}^{(z)}$.

Liquid crystals in general are known to be inhomogeneous and electrically anisotropic with source-free interior [11]. To model the propagation of light through such media, avoiding the spurious modes observed with equation (2.0.16) [39], we choose to work with the vector wave equation which we formalize next. In addition, the electrical properties of the domain are now expressed in terms of 3×3 symmetric tensors. The relative permittivity for example we be denoted as

$$\boldsymbol{\epsilon_r}(\mathbf{r}) = \begin{bmatrix} \epsilon_r^{xx} & \epsilon_r^{xy} & \epsilon_r^{xz} \\ \epsilon_r^{yx} & \epsilon_r^{yy} & \epsilon_r^{yz} \\ \epsilon_r^{zx} & \epsilon_r^{zy} & \epsilon_r^{zz} \end{bmatrix} \quad \text{for all} \quad \mathbf{r}(x,y,z) \in \Omega$$

In the conditions of the experiment we are investigating, the magnetic permeability tensor $\boldsymbol{\mu}$ is considered fixed and isotropic, while the electrical conductivity $\boldsymbol{\sigma}$ is negligibly small in the operating frequency, thus our main property of interest is the relative electric permittivity or dielectric tensor $\boldsymbol{\epsilon_r}$ which relates to the refractive index $\boldsymbol{n}$ of the material via

$$\boldsymbol{n}(\mathbf{r}) = \sqrt{\boldsymbol{\epsilon_r}(\mathbf{r})}$$

In a similar manner, applying the source and charge free conditions to the equation (2.0.14) for a domain of arbitrary electrical properties $\boldsymbol{\epsilon_r} > 0$ and $\mu_r > 0$ we arrive

at the *vector wave* equation with respect to the electric field, which is the main partial differential equation (pde) of the problem in consideration:

$$\frac{1}{\boldsymbol{\mu_r}}\nabla\times\nabla\times\mathbf{E}-k_0^2\boldsymbol{\epsilon_r}\mathbf{E}=0 \tag{2.0.17}$$

This elliptic pde has a non trivial solution under the influence of some boundary conditions. The appropriate boundary conditions that guarantee the uniqueness of the solution are those given by the uniqueness theorem which is stated next [17].

Theorem 2.0.1. *In a closed region Ω, completely occupied with dissipative media, the pair of the time-harmonic vector fields $(\mathbf{E},\mathbf{H})$ is uniquely determined by the impressed currents in the interior of Ω and the tangential components of the electric or magnetic field on the closed boundary $\partial\Omega$.*

Corollary 2.0.2. *In corollary of the above uniqueness theorem, if a harmonic field has zero tangential components of the electric or magnetic field on the boundary of the domain, then the field in its interior vanishes.*

2.1. **Function spaces and the variational formulation of the problem.** For the weak-variational formulation of the problem, we introduce the following Sobolev spaces for the variables of interest, following the notation of [3]. The Hilbert space $L^2(\Omega)^3$ denotes the vector space of all the square integrable scalar functions in Ω

$$L^2(\Omega)^3=\{u\cdot\int_\Omega |u|^2\,\mathrm{d}\Omega<\infty\} \tag{2.1.1}$$

while we the space $\mathbb{L}^2(\Omega)^3$ is that of all square integrable vector functions in the domain

$$\mathbb{L}^2(\Omega)^3=\{\mathbf{E}\cdot\int_\Omega |\mathbf{E}|^2\,\mathrm{d}\Omega<\infty\} \tag{2.1.2}$$

Using these definitions, for the scalar electrostatic or magneto-static potential we construct the space

$$L^2_{grad}(\Omega)^3=\{u\in L^2(\Omega)^3,\nabla u\in\mathbb{L}^2(\Omega)^3\} \tag{2.1.3}$$

where the Sobolev space $L^2_{grad}(\Omega)^3$ is an alternative notation for the Hilbert space $H^1(\Omega)^3$. For the electric and magnetic fields we introduce the appropriate vector spaces

$$\mathbb{L}^2_{curl}(\Omega)^3=\{\mathbf{E}\in\mathbb{L}^2(\Omega)^3,\nabla\times\mathbf{E}\in\mathbb{L}^2(\Omega)^3\} \tag{2.1.4}$$

and

$$\mathbb{L}^2_{curl}(\partial\Omega)^3=\{\mathbf{E}\in\mathbb{L}^2_{curl}(\Omega)^3,\hat{\mathbf{n}}\times\mathbf{E}=g\text{ on }\partial\Omega\} \tag{2.1.5}$$

The spaces $L^2(\Omega)^3$ are equipped with the inner products

$$\langle u,\phi\rangle_{L^2(\Omega)^3}=\int_\Omega u\,\overline{\phi}\,\mathrm{d}\Omega \tag{2.1.6a}$$

$\forall\, u,\phi\in L^2(\Omega)^3$, and

$$\langle\mathbf{E},\mathbf{F}\rangle_{\mathbb{L}^2_{curl}(\Omega)^3}=\int_\Omega\mathbf{E}\,\overline{\mathbf{F}}\,\mathrm{d}\Omega+\int_\Omega(\nabla\times\mathbf{E})\,(\overline{\nabla\times\mathbf{F}})\,\mathrm{d}\Omega \tag{2.1.6b}$$

$\forall\,\mathbf{E},\mathbf{F}\in\mathbb{L}^2_{curl}(\Omega)^3$ and the norms

$$\|u\|_{L^2(\Omega)^3}=\langle u,u\rangle^{1/2}_{L^2(\Omega)^3} \tag{2.1.7a}$$

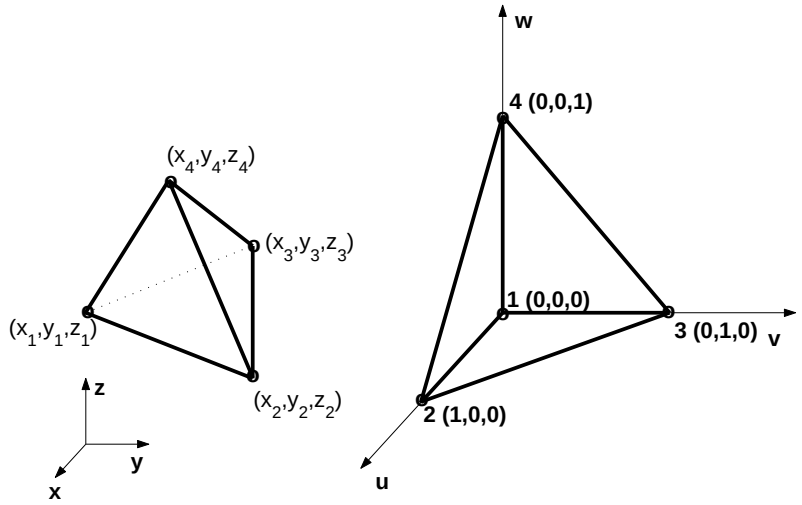

FIGURE 3. The isoparametric mapping from the master element in the local coordinate system $\mathcal{L}$ to the k'th element in global set of coordinates $\mathcal{G}$.

for the scalar functions, and

$$\|\mathbf{E}\|_{\mathbb{L}^2_{curl}(\Omega)^3} = \langle \mathbf{E}\,\mathbf{E}\rangle^{1/2}_{\mathbb{L}^2_{curl}(\Omega)^3} \tag{2.1.7b}$$

for the vector fields, where ϕ and $\mathbf{F}$ are the test functions associated with the electric scalar potential and the field respectively, while $\overline{\phi}$ and $\overline{\mathbf{E}}$ denote the corresponding complex conjugates. The electrical parameters of the domain are tensors and thus we will denote their space as a tensor product of two vector spaces such as $\mathbf{X} \subset \mathbb{L}^2(\Omega)^3 \otimes \mathbb{L}^2(\Omega)^3$. For clarity in our notation we introduce the spaces of complex vectors $\mathbf{Y}$ for the applied Neumann boundary components of $\{\mathbf{n}\times\mathbf{H}\}_{i=1}^q$ on $\partial\Omega$, and $\mathbf{Z}$ for the boundary measurements $\{\mathbf{n}\times\mathbf{E}_i\}_{i=1}^m$, where q the number of experiments performed and m the total number of measurements gathered.

Let $\Omega \subset \mathbb{R}^3$ be a Lipschitz domain with closed boundary $\partial\Omega$. In the high-frequency range, if no magnetic or electric sources are present inside the domain the governing elliptic partial differential equation derived from the time-harmonic space-frequency Maxwell's equations with respect to the electric field is

$$\begin{aligned} \nabla\times\Big(\frac{1}{\boldsymbol{\mu_r}}\nabla\times\mathbf{E}(\mathbf{r})\Big) - k_0^2\,\boldsymbol{\epsilon_r}\,\mathbf{E}(\mathbf{r}) = 0 \quad \mathbf{r}\in\Omega \\ \nabla\cdot\big(\epsilon_0\boldsymbol{\epsilon_r}\mathbf{E}(\mathbf{r})\big) = 0 \end{aligned} \tag{2.1.8a}$$

or in terms of the magnetic field

$$\begin{aligned} \nabla\times\Big(\frac{1}{\boldsymbol{\epsilon_r}}\nabla\times\mathbf{H}(\mathbf{r})\Big) - k_0^2\,\boldsymbol{\mu_r}\,\mathbf{H}(\mathbf{r}) = 0 \quad \mathbf{r}\in\Omega \\ \nabla\cdot\big(\mu_0\boldsymbol{\mu_r}\mathbf{H}(\mathbf{r})\big) = 0 \end{aligned} \tag{2.1.8b}$$

To derive the weak formulation we follow a Galerkin approach. Multiplying (2.1.8a) with an arbitrary test function $\mathbf{F} \in \mathbb{L}^2_{curl}(\Omega)^3$ and integrating over the

domain gives

$$\int_{\Omega} \Big\{ \mathbf{F} \cdot \nabla \times \Big(\frac{1}{\boldsymbol{\mu_r}} \nabla \times \mathbf{E} \Big) - \mathbf{F} \cdot k_0^2 \, \boldsymbol{\epsilon_r} \, \mathbf{E} \Big\} \, \mathrm{d}\Omega = 0 \tag{2.1.9}$$

and using the vector calculus identity

$$\mathbf{A} \cdot (\nabla \times \mathbf{B}) = (\nabla \times \mathbf{A}) \cdot \mathbf{B} - \nabla \cdot (\mathbf{A} \times \mathbf{B}) \tag{2.1.10}$$

we arrive at

$$\begin{aligned} \int_{\Omega} \big(\nabla \times \mathbf{F} \big) \cdot \big(\frac{1}{\boldsymbol{\mu_r}} \nabla \times \mathbf{E} \big) \, \mathrm{d}\Omega - \int_{\Omega} \nabla \cdot \Big(\mathbf{F} \times \big(\frac{1}{\boldsymbol{\mu_r}} \nabla \times \mathbf{E} \big) \Big) \, \mathrm{d}\Omega \\ - \int_{\Omega} \mathbf{F} \cdot k_0^2 \, \boldsymbol{\epsilon_r} \, \mathbf{E} \, \mathrm{d}\Omega = 0 \end{aligned} \tag{2.1.11}$$

Invoking the divergence theorem

$$\int_{\Omega} \nabla \cdot \mathbf{A} \, \mathrm{d}\Omega = \oint_{\partial\Omega} \mathbf{A} \cdot \hat{\mathbf{n}} \, \mathrm{ds} \tag{2.1.12}$$

and the vector calculus identity

$$(\mathbf{A} \times \mathbf{B}) \cdot \hat{\mathbf{n}} = -\mathbf{A} \cdot (\hat{\mathbf{n}} \times \mathbf{B}) \tag{2.1.13}$$

yields

$$\begin{aligned} \int_{\Omega} \Big(\frac{1}{\boldsymbol{\mu_r}} (\nabla \times \mathbf{F}) \cdot (\nabla \times \mathbf{E}) - k_0^2 \boldsymbol{\epsilon_r} \mathbf{F} \cdot \mathbf{E} \Big) \, \mathrm{d}\Omega \\ + \oint_{\partial\Omega} \mathbf{F} \cdot \Big(\hat{\mathbf{n}} \times \frac{1}{\boldsymbol{\mu_r}} \nabla \times \mathbf{E} \Big) \, \mathrm{ds} = 0 \end{aligned} \tag{2.1.14}$$

where $\hat{\mathbf{n}}$ is the normal outward unit vector at $\partial\Omega$. Substituting for the curl of the magnetic field from equation (2.0.11) into (2.1.14), yields the *variational formulation* of the problem, In this context, we seek to find the distribution of the electric field $\mathbf{E}(\mathbf{r}) \in \mathbb{L}^2_{curl}(\Omega)^3$ in the interior of a finite domain $\Omega \subset \mathbb{R}^3$ with electrical properties $\boldsymbol{\mu_r}$ and $\boldsymbol{\epsilon_r}$, so that the relations

$$\int_{\Omega} \Big(\frac{1}{\boldsymbol{\mu_r}} (\nabla \times \mathbf{F}) \cdot (\nabla \times \mathbf{E}) - k_0^2 \boldsymbol{\epsilon_r} \mathbf{F} \cdot \mathbf{E} \Big) \, \mathrm{d}\Omega = j k_0 Z_0 \oint_{\partial\Omega} \mathbf{F} \cdot \Big(\hat{\mathbf{n}} \times \mathbf{H} \Big) \, \mathrm{ds} = 0 \tag{2.1.15a}$$

$$\nabla \cdot \big(\epsilon_0 \boldsymbol{\epsilon_r} \mathbf{E}(\mathbf{r}) \big) = 0 \qquad \mathbf{r} \in \Omega \tag{2.1.15b}$$

$$\hat{\mathbf{n}} \times \mathbf{H}(\mathbf{r}) = g \quad \mathbf{r} \in \partial\Omega \tag{2.1.15c}$$

hold for all $\mathbf{F} \in \mathbb{L}^2_{curl}(\Omega)^3$, given the frequency of the applied signal ω and the distribution of the tangential component of the magnetic field at the boundary g. The problem (2.1.15) has a unique solution for $\boldsymbol{\epsilon_r} > 0$.

3. Finite elements

In their book Volakis et al. [39] quote that the order of the differential equation to be solved determines the order of the shape function to be used in the Galerkin formulation. For elliptic PDEs of order $2k$, with $k = 1, 2, \ldots$, the continuity requirement is C^{k-1}. In effect, for the electromagnetic problem in (2.1.8) C^0 continuous functions are often used since the discontinuous first derivatives are piecewise integrable. Nodal based shape functions (of the Lagrange family) or Whitney 0-forms derived in triangles and tetrahedra are C^0 continuous across the element interfaces.

Whitney form	Element type	Elliptic PDE operator	Continuity
W^0	Nodal elements	grad	C^0 function cont.
W^1	Edge elements	curl	tangential component
W^2	Face elements	div	normal component

TABLE 1. The continuity requirements for shape functions used in computational electromagnetic problems.

In contrast, edge or Nedélec shape functions, or Whitney 1-forms, maintain continuity only in their tangential component of the, thus allowing the normal component of the field to be discontinuous across the inter-element interfaces. This makes them well equipped to approximate the behavior exhibited by electromagnetic fields in highly anisotropic domains. Moreover, face shape functions or Whitney 2-forms, have their normal component continuous in the domain of interest.

For the derivation of the finite element method we use three-dimensional simplices, or linear tetrahedral similar to those appearing in figure 3. For the isoparametric mapping we use two sets of coordinates. The k'th simplex in the model is positioned in the global coordinates $\mathcal{G}(x, y, z)$, while the local-master element is located in the local coordinates $\mathcal{L}(u, v, w)$, as indicated in the figure. For the local-global mapping, functions defined on elements in $\mathcal{G}$ can be transformed to functions on the master element in $\mathcal{L}$ using the coordinate transformation formulae

$$\begin{aligned} x(u,v,w) &= \sum_{i=1}^{4} x_i N_i(u,v,w) \\ y(u,v,w) &= \sum_{i=1}^{4} y_i N_i(u,v,w) \\ z(u,v,w) &= \sum_{i=1}^{4} z_i N_i(u,v,w) \end{aligned} \tag{3.0.16}$$

where the linear nodal Lagrangian shape functions $N_i \in L^2_{grad}(\Omega)^3$ for the master simplex are defined as

$$\begin{aligned} N_1(u,v,w) &= 1 - u - v - w \\ N_2(u,v,w) &= u \\ N_3(u,v,w) &= v \\ N_4(u,v,w) &= w \end{aligned} \tag{3.0.17}$$

resembling the barycentric coordinates on the standard tetrahedron, and satisfying $\sum_{i=1}^{4} N_i = 1$. On the k'th element in $\mathcal{G}$, the shape functions are defined as

(3.0.18)

$$N_1(x,y,z) = \frac{1}{6V}\begin{vmatrix} 1 & x & y & z \\ 1 & x_2 & y_2 & z_2 \\ 1 & x_3 & y_3 & z_3 \\ 1 & x_4 & y_4 & z_4 \end{vmatrix}, \; N_2(x,y,z) = \frac{1}{6V}\begin{vmatrix} 1 & x_1 & y_1 & z_1 \\ 1 & x & y & z \\ 1 & x_3 & y_3 & z_3 \\ 1 & x_4 & y_4 & z_4 \end{vmatrix}$$

$$N_3(x,y,z) = \frac{1}{6V}\begin{vmatrix} 1 & x_1 & y_1 & z_1 \\ 1 & x_2 & y_2 & z_2 \\ 1 & x & y & z \\ 1 & x_4 & y_4 & z_4 \end{vmatrix}, \; N_4(x,y,z) = \frac{1}{6V}\begin{vmatrix} 1 & x_1 & y_1 & z_1 \\ 1 & x_1 & y_1 & z_1 \\ 1 & x_3 & y_3 & z_3 \\ 1 & x & y & z \end{vmatrix}$$

where V is the volume of the k'th tetrahedron. Having defined the nodal shape functions we can proceed to the definition of the standard basis of linear *edge* shape functions $\{\mathbf{L}_i\}_{i=1}^{ne}$ defined on each edge of the model as

$$\mathbf{L}_i = l_i \left(N_m^i \nabla N_n^i - N_n^i \nabla N_m^i\right) \quad i = 1 : ne, \;\; \text{and } n, m \in V \tag{3.0.19}$$

where l_i is the length of the i'th edge, N_n^i, N_n^i are the definitions of the nodal shape functions at the two vertices across the edge, and V is the set of indices for the nodes in the model. It must also be quoted that vector finite elements have magnitude as well as direction, thus the shape function in (3.0.19) is defined from the vertex m towards the vertex n. The selection of the particular class of basis functions has some important properties. They have a constant tangential component upon the edge on which they are defined. This is convenient for the boundary conditions we seek to apply, e.g. tangential components of the magnetic field on a subset of the boundary. They are divergence-free and hence they satisfy by default the gauge conditions of the problem as in (2.1.8), hence avoiding the spurious modes observed in the solution of the scalar wave equation. From the definition (3.0.19) it is clear that the edge elements are divergence free

$$\nabla \cdot \mathbf{L}_i = \nabla \cdot (N_m^i \nabla N_n^i) - \nabla \cdot (N_n^i \nabla N_m^i) = 0 \tag{3.0.20}$$

hence satisfy by default the gauge conditions in (2.1.8). Moreover if $\hat{\mathbf{e}}_i$ is the unit tangent vector on the edge i pointing to the direction of the shape function, it is easy to show that $\mathbf{L}_i$ has a constant (unit) tangential component along the i'th edge

$$\hat{\mathbf{e}}_i \cdot \mathbf{L}_i = \big((N_m^i + N_n^i)/l_i\big) l_i = 1 \qquad i = 1 : ne \tag{3.0.21}$$

To derive the finite element formulation of the problem the domain Ω is discretized in linear tetrahedra, effectively approximating the infinite dimensional space $\mathbb{L}^2_{curl}(\Omega)^3$ with a sequence of finite dimensional subspaces $\mathbb{L}^2_{curl}(\Omega_h)^3$. Using this subspace, the electric field in the discrete model of the computational domain can be expanded as

$$\mathbf{E}_h = \sum_{i=1}^{ne} E_i \, \mathbf{L}_i \tag{3.0.22}$$

where $\mathbf{E}_h \in \mathbb{L}^2_{curl}(\Omega_h)^3$, E_i is the tangential component of the electric field on the i'th edge, and ne is the total number of edges in the mesh. Introducing the definition (3.0.22) into the weak formulation and if no electric or magnetic sources

are present, the *finite element formulation* of the problem is to find the electric field $\mathbf{E}_h \in \mathbb{L}^2_{curl}(\Omega_h)^3$ so that

$$\int_\Omega \Big(\frac{1}{\boldsymbol{\mu_r}} (\nabla \times \mathbf{F}) \cdot (\nabla \times \mathbf{E}_h) - k_0^2 \boldsymbol{\epsilon_r} \mathbf{F} \cdot \mathbf{E}_h \Big) \, \mathrm{d}\Omega = jk_0 Z_0 \oint_{\partial\Omega} \big(\hat{\mathbf{n}} \times \mathbf{H} \big) \cdot \mathbf{F} \, \mathrm{ds} \tag{3.0.23a}$$

$$\nabla \cdot \big(\boldsymbol{\epsilon_r}(\mathbf{r}) \mathbf{E}_h(\mathbf{r}) \big) = 0 \quad \mathbf{r} \in \Omega \tag{3.0.23b}$$

$$\hat{\mathbf{n}} \times \mathbf{H}(\mathbf{r}) = g \quad \mathbf{r} \in \partial\Omega \tag{3.0.23c}$$

for all $\mathbf{F} \in \mathbb{L}^2_{curl}(\Omega_h)^3$.

3.1. **Boundary conditions.** From the the weak formulation (2.1.15) as well as from the finite element formulation (3.0.23) it becomes apparent that for the problem to yield a unique nonzero solution it requires the knowledge of the tangential components of either field on the surface of the domain, or a relation between the two. The first option is rather unrealistic since there are no means by which we can measure the complete set of Dirichlet (tangential of electric field) or Neumann (tangential of magnetic field) data for the pde (2.1.8a). The second option is somewhat more realistic and it is sometimes employed in the context of the Letonovic boundary condition, also known as surface impedance boundary condition (SIBC) in antenna and microwave engineering systems [17, 39].

The boundary conditions we seek to apply for this problem is the knowledge of the Berreman vector ψ^b at entering the model through a small subset of the boundary $\Gamma_1 \subset \partial\Omega$. Realistically though, the excitation conditions we acquire are actually known at a small distance outside the computational domain, e.g. where the source of polarized light is places, thus to be able to enforce the boundary conditions relations that couple near-field 'actual' excitation conditions to those which describe the fields at the incident point on Γ_1 are required. The knowledge of $\psi^b(\mathbf{r})$ at Γ_1 provides the opportunity to work with either Dirichlet or Neumann data, and here we choose to enforce Neumann boundary conditions. In order to achieve this a surface expansion of the magnetic field at the boundary of the domain must be introduced, thus if $\{\mathbf{Q}_i\}_{i=1}^{ns}$ is a basis of linear edge shape functions spanning over the boundary edges of the model, the surface magnetic field is approximated as

$$\mathbf{H}_{\mathbf{s}h} = \sum_{i=1}^{ns} H_i \mathbf{Q}_i \tag{3.1.1}$$

with $\mathbf{H}_{\mathbf{s}h} \in \mathbb{L}^2_{curl}(\partial\Omega_h)^3$ and ns the total number of boundary edges. The proposed methodology shares various similarities with the technology traditionally used in far-field wave propagation, antenna and scattering problems, although no artificial boundary is needed to truncate the computational domain. As in many microwave and antenna problems we use an integral equation to relate the tangential components of the two fields at the boundary, hence the hybrid technology of finite elements with boundary integral equations is known as *Finite Element - Boundary Integral* method (FEBI). The specific boundary condition to be enforced is known as *Magnetic Field Integral Equation* (MFIE) which is an integral form of a Neumann boundary condition. The derivation of the FEBI method is based on the surface equivalence principle, which we state next for completeness.

Theorem 3.1.1. *The sources that produce the same field within a region are said to be equivalent within that region. In this case, the field exterior to the boundaries of the model may be exactly represented by equivalent currents placed on its boundary. These are given in terms of the exterior electromagnetic fields as*

$$\mathbf{J_s}(\mathbf{r},\omega) = \hat{\mathbf{n}} \times \mathbf{H}^{ext} \quad \text{and} \quad \mathbf{M_s}(\mathbf{r},\omega) = \mathbf{E}^{ext} \times \hat{\mathbf{n}} \qquad \forall\, \mathbf{r} \in \partial\Omega \tag{3.1.2}$$

where $\mathbf{H}^{ext}$ *and* $\mathbf{E}^{ext}$ *are taken on the external side of the boundary* $\partial\Omega^{+}$.

4. Finite Element Boundary Integral method

A closer look at the system of equations (3.0.23a) reveals its underdetermined status. The reason for this is that while the test functions $\mathbf{F}$ are exclusively associated with the electric field in the closure of the domain, both $\mathbf{E}$ in $\overline{\Omega}$ and $\mathbf{H}$ in $\partial\Omega$ are to be evaluated. To resolve this, more equations must be imported into the system in order to guarantee the uniqueness of the solution. To formulate the required equations we attempt to model how the magnetic field at the surface relates to the applied excitation conditions just outside the boundary of the domain. More precisely, for a plane wave travelling impinging the surface of the domain, the exterior excitation is given by

$$\mathbf{H}^{ext} = \mathbf{H}^{i} + \mathbf{H}^{r} + \mathbf{H}^{s} \tag{4.0.3}$$

where the overall external magnetic field is expressed as the sum of the incident $\mathbf{H}^{i}$, the reflected $\mathbf{H}^{r}$ and the scattered $\mathbf{H}^{s}$ components of the magnetic field at the boundary. Using the surface equivalence theorem $\mathbf{H}^{s}$ can be expressed in terms of the surface equivalence current densities $\mathbf{J_s}$ and $\mathbf{M_s}$, and (4.0.3) can be cast as a 'magnetic field integral equation' (MFIE)

$$\begin{aligned} -\hat{\mathbf{n}} \times (\mathbf{H}^{i}(\mathbf{r}) + \mathbf{H}^{r}(\mathbf{r})) = &-\frac{\mathbf{J_s}(\mathbf{r})}{2} - \oint_{S'} \hat{\mathbf{n}} \times (\nabla \times \mathbf{G}(\mathbf{r},\mathbf{r}')) \cdot \mathbf{J_s}(\mathbf{r}')\, \mathrm{d}s' \\ &+ jk_0 Y_0 \oint_{S'} \hat{\mathbf{n}} \times \mathbf{G}(\mathbf{r},\mathbf{r}') \cdot \mathbf{M_s}(\mathbf{r}')\, \mathrm{d}s' \end{aligned} \tag{4.0.4}$$

valid for closed scattering surfaces S. In the original notation of the MFIE the first term on the right hand side is $-\mathbf{J_s}$ and the integral immediately after is a Cauchy integral. The simplified version given here is due to the fact that A.J. Poggio and E.K. Miller have proved that the difference between the principal value of the surface integral and the total value of the integral is $\mathbf{J_s}/2$. For finite models in the near-field approximation, Green's function can be replaced with a free-space dyadic Green's function $\mathbf{G}(\mathbf{r},\mathbf{r}')$,

$$\mathbf{G}(\mathbf{r},\mathbf{r}') = \Big(\boldsymbol{I} + \frac{\nabla\nabla}{k_0^2}\Big) G(\mathbf{r},\mathbf{r}') \tag{4.0.5}$$

whose curl is related to the gradient of the scalar Green's function via the identity

$$\nabla \times \mathbf{G}(\mathbf{r},\mathbf{r}') = -\nabla G(\mathbf{r},\mathbf{r}') \times \boldsymbol{I} \tag{4.0.6}$$

In the above, $\boldsymbol{I}$ is the unit dyad tensor, R is the distance between observation (field) point $\mathbf{r}$ and integration (source) point $\mathbf{r}'$, and the scalar Green's function for $\mathbf{r} \neq \mathbf{r}'$ is given by

$$G(\mathbf{r},\mathbf{r}') = \frac{e^{-jk_0 R}}{4\pi R} \tag{4.0.7}$$

with gradient

$$\nabla G(\mathbf{r},\mathbf{r}') = -\nabla' G(\mathbf{r},\mathbf{r}') = -\Big(jk_0 + \frac{1}{R}\Big)\frac{e^{-jk_0R}}{4\pi R}\hat{\mathbf{R}} \tag{4.0.8}$$

where the unit vector $\hat{\mathbf{R}} = (\mathbf{r}-\mathbf{r}')/R$ and $R = \|\mathbf{R}\| = |\mathbf{r}-\mathbf{r}'|$. In the above the differential operators $\nabla, \nabla\cdot$ and $\nabla\times$ are with respect to $\mathbf{r}$ and $\nabla', \nabla'\cdot$ and $\nabla'\times$ are with respect to the source variable $\mathbf{r}'$. Using these identities and some trivial algebra the MFIE can be written in a compact form as

$$-\hat{\mathbf{n}}\times(\mathbf{H}^i(\mathbf{r}) + \mathbf{H}^r(\mathbf{r})) = -\frac{\mathbf{J_s}(\mathbf{r})}{2} - \hat{\mathbf{n}}\times\mathbf{K}(\mathbf{J_s}) - \hat{\mathbf{n}}\times\mathbf{L}(\mathbf{M_s}) \tag{4.0.9}$$

where the integral operators are given by

$$\mathbf{K}(\mathbf{J_s}) = \oint_{S'} \mathbf{J_s}(\mathbf{r}')\times\nabla G(\mathbf{r},\mathbf{r}')\,\mathrm{ds}' \tag{4.0.10a}$$

$$\mathbf{L}(\mathbf{M_s}) = jk_0Y_0\oint_{S'}\Big(\mathbf{M_s}(\mathbf{r}')G(\mathbf{r},\mathbf{r}') + \frac{1}{k_0^2}\nabla'\cdot\mathbf{M_s}(\mathbf{r}')\,\nabla G(\mathbf{r},\mathbf{r}')\Big)\,\mathrm{ds}' \tag{4.0.10b}$$

When working with the MFIE care must be taken since the integral operator $\mathbf{L}$ becomes singular at the resonant frequencies of the liquid crystal, causing the formulation to yield spurious forward solutions since the operator has a nonempty null space. This problem can be avoided by carefully selecting to work at a non-resonant frequency range or by formulating the combined field integral equations (CFIE) as suggested by Jin [17] and Tzoulis et al. [38] , effectively resulting in an integral operator whose resonant frequencies are strictly complex. As the finite element formulation (3.0.23) involves the fields in the closure of the domain, while those in the boundary integral (4.0.4) refer to the outer region, these must be coupled together in order to combine in a system of equations with a unique solution. This is done by enforcing tangential continuity of the fields across the boundary of the computational domain. In particular,

(4.0.11)

$$\begin{aligned}
\hat{\mathbf{n}}\times\big[\nabla\times\mathbf{E}(\mathbf{r})\big]\Big|_{\mathbf{r}\in\partial\Omega^-} &= \hat{\mathbf{n}}\times\big[\frac{1}{\mu_r}\nabla\times\mathbf{E}^{ext}(\mathbf{r})\big]\Big|_{\mathbf{r}\in\partial\Omega^+} \quad \text{(tangential H continuity)}\\
\hat{\mathbf{n}}\times\mathbf{E}(\mathbf{r})\Big|_{\mathbf{r}\in\partial\Omega^-} &= \hat{\mathbf{n}}\times\mathbf{E}^{ext}(\mathbf{r})\Big|_{\mathbf{r}\in\partial\Omega^+} \quad \text{(tangential E continuity)}
\end{aligned}$$

where $\partial\Omega^-$, $\partial\Omega^+$ refer to the inner/internal and outer/external side of the boundary, hence the fields on the left hand side of the equations in (4.0.11) without the subscript are those in the closure of the domain. The continuity condition associated with the magnetic field (in this formulation a natural boundary condition) is implicitly enforced allowing

$$\mathbf{H}^{ext}(\mathbf{r})\Big|_{\mathbf{r}\in\partial\Omega^+} = \mathbf{H}(\mathbf{r})\Big|_{\mathbf{r}\in\partial\Omega^-} \tag{4.0.12}$$

as long as the essential boundary condition for the electric field is explicitly imposed in the formulation. Applying the Galerkin method on the integral equation (4.0.4)

and using the relations in the equivalence principle (3.1.2) yields

(4.0.13a)
$$
\begin{aligned}
&-\frac{1}{2}\oint_S \mathbf{T}(\mathbf{r})\cdot\big(\hat{\mathbf{n}}(\mathbf{r})\times\mathbf{H}_{\mathbf{s}h}(\mathbf{r})\big)\,\mathrm{ds}\\
&-\oint_S \mathbf{T}(\mathbf{r})\cdot\hat{\mathbf{n}}(\mathbf{r})\times\Big(\oint_{S'}\nabla' G(\mathbf{r},\mathbf{r}')\times\big(\hat{\mathbf{n}}(\mathbf{r}')\times\mathbf{H}_{\mathbf{s}h}(\mathbf{r}')\big)\,\mathrm{ds}'\Big)\,\mathrm{ds}\\
&+jk_0Y_0\oint_S \mathbf{T}(\mathbf{r})\cdot\hat{\mathbf{n}}(\mathbf{r})\times\Big(\oint_{S'}\big(\hat{\mathbf{n}}(\mathbf{r}')\times\mathbf{E}_{\mathbf{s}h}(\mathbf{r}')\big)\,G(\mathbf{r},\mathbf{r}')\,\mathrm{ds}'\Big)\mathrm{ds}\\
&-j\frac{Y_0}{k_0}\oint_S \mathbf{T}(\mathbf{r})\cdot\hat{\mathbf{n}}(\mathbf{r})\times\Big(\oint_{S'}\nabla'\cdot\big(\hat{\mathbf{n}}(\mathbf{r}')\times\mathbf{E}_{\mathbf{s}h}(\mathbf{r}')\big)\,\nabla' G(\mathbf{r},\mathbf{r}')\,\mathrm{ds}'\Big)\,\mathrm{ds}\;=\;\psi^{ext}
\end{aligned}
$$

where $\mathbf{E}_{\mathbf{s}h}$ is the subset of $\mathbf{E}_h$ restricted on the boundary of the domain, the exterior excitation term ψ^{ext} is given by

$$
\psi^{ext} = -jk_0Z_0\oint_S \mathbf{T}(\mathbf{r})\cdot\big(\hat{\mathbf{n}}(\mathbf{r})\times(\mathbf{H}^i+\mathbf{H}^r)\big)\,\mathrm{ds} \tag{4.0.13b}
$$

The vector functions $\mathbf{T}\in\mathbb{L}^2_{curl}(\partial\Omega_h)^3$ are the test functions for the surface magnetic field and have support restricted on the boundary edges of the domain. In the double integrals of (4.0.13) above notice that the inner integral is evaluated at the source triangle S' whose unit outward normal is denoted by $\hat{\mathbf{n}}(\mathbf{r})$, while the outer integral is evaluated on the observation triangle S with unit normal $\hat{\mathbf{n}}(\mathbf{r}')$. In the system of equations (4.0.13) there are three field unknowns, namely the interior electric field $\mathbf{E}$, the exterior or surface electric field $\mathbf{E}^{ext}$ and the exterior or surface magnetic field $\mathbf{H}^{ext}$. We can now proceed to impose the continuity of the two fields at the boundary as in equation (4.0.11). To enforce the continuity in the tangential component of the magnetic field outside and at the boundary of the domain we use (4.0.12), which constitutes to the mere assumption that the magnetic field at the point of incidence on the boundary is the same to the magnetic field at a point just before the boundary. In order to impose the continuity on the electric field we explicitly set the shape functions for $\mathbf{E}_{\mathbf{s}h}$ and $\mathbf{E}^{ext}_h$ to be the same. Hence if the exterior electric field can be expressed as a linear combination of the basis $\{\boldsymbol{\Xi}_i\}_{i=1}^{ns}$ for $\boldsymbol{\Xi}_i\in\mathbb{L}^2_{curl}(\partial\Omega_h)^3$, then we set

$$
\{\boldsymbol{\Xi}\}_{i=1}^{ns}=\{\mathbf{L}\}_{i=1}^{ns}\quad\Longrightarrow\quad \mathbf{E}_{\mathbf{s}h}(\mathbf{r})\Big|_{\mathrm{r}\in\partial\Omega^+}=\mathbf{E}^{ext}_h(\mathbf{r})\Big|_{\mathbf{r}\in\partial\Omega^-} \tag{4.0.14}
$$

Using the expansions for $\mathbf{E}_h$ and $\mathbf{H}_{\mathbf{s}h}$ and setting $\mathbf{F}=\mathbf{L}_i\in\mathbb{L}^2_{curl}(\Omega)^3$ leads to the *finite element formulation* of the problem

$$
\begin{aligned}
\sum_{n=1}^{ne}\Big\langle\nabla\times\mathbf{L}_m,\frac{1}{\boldsymbol{\mu_r}}\nabla\times\mathbf{L}_n\Big\rangle_{L^2(\Omega)^3}&-k_0^2\Big\langle\mathbf{L}_m,\boldsymbol{\epsilon_r}\mathbf{L}_n\Big\rangle_{L^2(\Omega)^3}\\
&=\sum_{n=1}^{ns}jk_0Z_0\oint_S\mathbf{L}_m\cdot\big(\hat{\mathbf{n}}(\mathbf{r})\times\mathbf{L}_n\big)\,\mathrm{ds}
\end{aligned} \tag{4.0.15a}
$$

for $m=1:ne$. If the basis functions for the magnetic field are chosen to be identical to those for the electric (although it is not imperative for the FEBI method), and use their tangential components as test functions, for the required surface integrals

are

(4.0.15b)

$$
\begin{aligned}
&-\sum_{n=1}^{ns}\frac{1}{2}\oint_S\big(\hat{\mathbf{n}}(\mathbf{r})\times\mathbf{L}_m(\mathbf{r})\big)\cdot\big(\hat{\mathbf{n}}(\mathbf{r})\times\mathbf{L}_n(\mathbf{r})\big)\,\mathrm{ds}\\
&-\sum_{n=1}^{ns}\oint_S\big(\hat{\mathbf{n}}(\mathbf{r})\times\mathbf{L}_m(\mathbf{r})\big)\cdot\hat{\mathbf{n}}(\mathbf{r})\times\oint_{S'}^{c}\Big(\nabla' G(\mathbf{r},\mathbf{r}')\times\big(\hat{\mathbf{n}}(\mathbf{r}')\times\mathbf{L}_n(\mathbf{r}')\big)\Big)\,\mathrm{ds}'\,\mathrm{ds}\\
&+jk_0Y_0\sum_{n=1}^{ns}\oint_S\big(\hat{\mathbf{n}}(\mathbf{r})\times\mathbf{L}_m(\mathbf{r})\big)\cdot\hat{\mathbf{n}}(\mathbf{r})\times\oint_{S'}\big(\mathbf{n}(\mathbf{r}')\times\mathbf{L}_n(\mathbf{r}')\big)\,G(\mathbf{r},\mathbf{r}')\,\mathrm{ds}'\,\mathrm{ds}\\
&-j\frac{Y_0}{k_0}\sum_{n=1}^{ns}\oint_S\big(\hat{\mathbf{n}}(\mathbf{r})\times\mathbf{L}_m(\mathbf{r})\big)\cdot\hat{\mathbf{n}}(\mathbf{r})\times\\
&\qquad\qquad\oint_{S'}\nabla'\cdot\big(\mathbf{n}(\mathbf{r}')\times\mathbf{L}_n(\mathbf{r}')\big)\,\nabla' G(\mathbf{r},\mathbf{r}')\,\mathrm{ds}'\,\mathrm{ds}=\psi^{ext}
\end{aligned}
$$

for $m=1:ns$. The reason for choosing this class of test functions for the MFIE will become apparent in the next section. Adopting this approach we can write two equations, each one involving the electric field in the closure of the domain and the magnetic field at the surface of the domain, for the interior and the exterior of the domain.

We begin with the *interior electric field testing* equation which we can write in matrix notation as

$$\mathbf{A}\,E+\mathbf{B}H=\psi^{int} \tag{4.0.16}$$

where E and H are the finite element coefficients in (3.0.22) and (3.1.1), $\mathbf{A}\in\mathbb{R}^{ne\times ne}$ is a real sparse matrix with entries

$$A_{m,n}=\int_\Omega\Big(\frac{1}{\boldsymbol{\mu_r}}(\nabla\times\mathbf{L}_m)(\nabla\times\mathbf{L}_n)-k_0^2\boldsymbol{\epsilon_r}\mathbf{L}_m\cdot\mathbf{L}_n\Big)\,\mathrm{d}\Omega \tag{4.0.17}$$

for $m,n=1:ne$, and $\mathbf{B}\in\mathbb{C}^{ne\times ns}$ a sparse matrix given by

$$B_{m,n}=-jk_0Z_0\oint_S\mathbf{L}_m\cdot(\hat{\mathbf{n}}\times\mathbf{L}_n)\,\mathrm{ds} \tag{4.0.18}$$

for $m=1:ne$ and $n=1:ns$. Finally, as no interior charges or sources are present within the liquid crystal $\psi^{int}=\mathbf{0}$ is a $ne\times 1$ zeros vector. The second equation is that of the *exterior surface magnetic field testing* which in a similar fashion we can write in a matrix notation as

$$\mathbf{C}H+\mathbf{D}E=\psi^{ext} \tag{4.0.19}$$

where $\mathbf{C}\in\mathbb{C}^{ns\times ns}$ is a dense matrix with complex entries given by

$$\mathbf{C}_{m,n}=\mathbf{C^1}_{m,n}+\mathbf{C^2}_{m,n} \tag{4.0.20a}$$

for $m,n=1:ns$ where

(4.0.20b)

$$
\begin{aligned}
\mathbf{C^1}_{m,n}&=-\frac{1}{2}\oint_S(\hat{\mathbf{n}}\times\mathbf{L}_m)\cdot(\hat{\mathbf{n}}\times\mathbf{L}_n)\,\mathrm{ds}\\
\mathbf{C^2}_{m,n}&=-\oint_S(\hat{\mathbf{n}}\times\mathbf{L}_m(\mathbf{r}))\cdot\Big(\hat{\mathbf{n}}(\mathbf{r})\times\oint_{S'}\nabla' G(\mathbf{r},\mathbf{r}')\times\big(\hat{\mathbf{n}}(\mathbf{r}')\times\mathbf{L}_n(\mathbf{r}')\big)\,\mathrm{ds}'\Big)\,\mathrm{ds}
\end{aligned}
$$

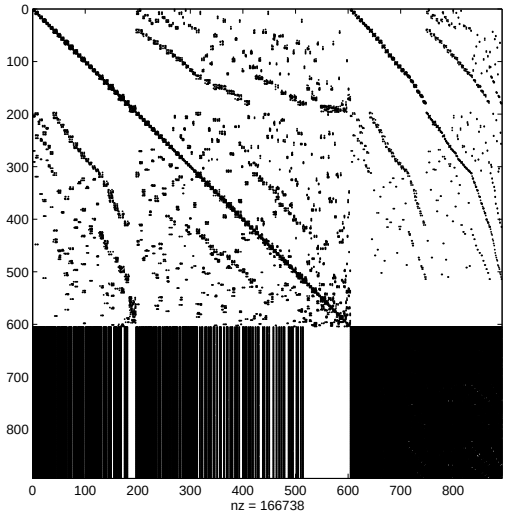

FIGURE 4. Sparsity plot of the FEBI system matrix indicating the sparse finite element and the dense boundary integral components. The matrix refers to a model with a total of 604 edges, out of which 288 lie on the boundary.

Note that the integrants in the single surface integrals are considered at the observation triangle only, so they are functions of the observation space variable $(\mathbf{r})$, while at the double integrals functions of both $(\mathbf{r})$ and $(\mathbf{r}')$ appear hence we use the extra notation to distinguish between them and enhance clarity. The matrix $\mathbf{D} \in \mathbb{C}^{ns \times ne}$ is also a dense matrix whose entries are given by the surface integrals

(4.0.21)

$$\mathbf{D}_{m,n} = jk_0 Y_0 \oint_S \big(\hat{\mathbf{n}} \times \mathbf{L}_m(\mathbf{r})\big) \cdot \hat{\mathbf{n}}(\mathbf{r}) \times \oint_{S'} \Big[\big(\hat{\mathbf{n}}(\mathbf{r}') \times \mathbf{L}_n(\mathbf{r}')\big)\, G(\mathbf{r}, \mathbf{r}') - \frac{1}{k_0^2} \Big(\nabla' \cdot \big(\hat{\mathbf{n}}(\mathbf{r}') \times \mathbf{L}_n(\mathbf{r}')\big)\, \nabla' G(\mathbf{r}, \mathbf{r}') \Big) \Big] \, \mathrm{ds}' \, \mathrm{ds}$$

for $m = 1 : ns$ and $n = 1 : ne$. Combining the two matrix equations we arrive in a system of $nt = ne + ns$ equations and nt unknowns

$$\begin{bmatrix} \mathbf{A} & \mathbf{B} \\ \mathbf{D} & \mathbf{C} \end{bmatrix} \begin{bmatrix} E \\ H \end{bmatrix} = \begin{bmatrix} \mathbf{0} \\ \psi^{ext} \end{bmatrix} \tag{4.0.22}$$

From the equations describing the integrals required for the forward computations, it is clear that the fem parts of the system matrix in (4.0.22), namely A, B, are sparse, whilst the boundary integral compartments C and D are dense. This is graphically illustrated in figure 4 that refers to a system with 604 edges out of which 288 are located at the boundary.

4.1. **Singularity in the surface integrals.** In evaluating the entries for the matrices $\mathbf{C}$ and $\mathbf{D}$ one should come across situations where the integrants become singular functions. This is due to the Green's function and its derivatives as these are involved in the above equations, which become asymptotically singular as the

distance between the observation and integration points goes to zero. In this section we describe the singular behavior in these integrants as $R \to 0$ and derive the methodology necessitated to treat the singularity and extract accurate estimates on the surface integrals required in (4.0.22). In particular, splitting the singular integral $\mathbf{D}$ into $\mathbf{D^1}$ and $\mathbf{D^2}$, so that $\mathbf{D} = \mathbf{D^1} + \mathbf{D^2}$ we have

$$\begin{aligned} \mathbf{D^1}_{m,n} = jk_0 Y_0 \oint_S \big(\hat{\mathbf{n}} \times \mathbf{L}_m(\mathbf{r})\big) \cdot \hat{\mathbf{n}}(\mathbf{r}) \times \\ \Big(\oint_{S'} G(\mathbf{r},\mathbf{r}') \, \big(\hat{\mathbf{n}}(\mathbf{r}') \times \mathbf{L}_n(\mathbf{r}')\big) \, \mathrm{ds}' \Big) \, \mathrm{ds} \end{aligned} \tag{4.1.1}$$

and

$$\begin{aligned} \mathbf{D^2}_{m,n} = -j \frac{Y_0}{k_0} \oint_S \big(\hat{\mathbf{n}} \times \mathbf{L}_m(\mathbf{r})\big) \cdot \hat{\mathbf{n}}(\mathbf{r}) \times \\ \Big(\oint_{S'} \Big(\nabla' \cdot \big(\hat{\mathbf{n}}(\mathbf{r}') \times \mathbf{L}_n(\mathbf{r}')\big) \, \nabla' G(\mathbf{r},\mathbf{r}') \Big) \, \mathrm{ds}' \Big) \, \mathrm{ds} \end{aligned} \tag{4.1.2}$$

As the edge shape functions $\mathbf{L}_m$ (and $\mathbf{Q}_n$) and their tangential surface components are in this case linear, their divergence is constant, hence the integral above can be further simplified to

$$\begin{aligned} \mathbf{D^2}_{m,n} = -j \frac{Y_0}{k_0} \oint_S \big(\hat{\mathbf{n}} \times \mathbf{L}_m(\mathbf{r})\big) \cdot \hat{\mathbf{n}}(\mathbf{r}) \times \\ \Big(\nabla' \cdot \big(\hat{\mathbf{n}}(\mathbf{r}') \times \mathbf{L}_n(\mathbf{r}')\big) \oint_{S'} \nabla' G(\mathbf{r},\mathbf{r}') \, \mathrm{ds}' \Big) \, \mathrm{ds} \end{aligned} \tag{4.1.3}$$

where the divergence of $\mathbf{E}$, and thus its shape and test functions, is independent of the coordinate system and therefore $\nabla \cdot \mathbf{E}(\mathbf{r}) = \nabla' \cdot \mathbf{E}(\mathbf{r}')$. As the integrals $\mathbf{D^1}$ and $\mathbf{D^2}$ involve only the scalar Green's function, for $R \to 0$ these are known to become $(1/R)$ singular. This form of singularity causes low-order numerical integration rules to fail in approximating the values of the above integrals, as Gaussian quadrature rules are most suited for smooth functions. Conventionally, see [34], [39] and [17] the singular integrals are treated by extracting one singular term from the kernel of Green's function, such as

$$G(\mathbf{r},\mathbf{r}') = \Big\{ \frac{e^{-jk_0 R}}{4\pi R} - \frac{1}{4\pi R} \Big\} + \frac{1}{4\pi R} \tag{4.1.4}$$

leaving a 'rather smooth' function, inside the braces, to be integrated numerically, where

$$\lim_{R \to 0} \Big\{ \frac{e^{-jk_0 R}}{4\pi R} - \frac{1}{4\pi R} \Big\} = \frac{-jk_0}{4\pi}$$

while the singular term is integrated using analytic formulae. In effect, for $R \to 0$ the integration is split as

$$\oint_{S'} \frac{e^{-jk_0 R}}{R} \, \mathrm{ds}' = \oint_{S'} \frac{e^{-jk_0 R} - 1}{R} \, \mathrm{ds}' + \oint_{S'} \frac{1}{R} \, \mathrm{ds}' \tag{4.1.5}$$

However, recent studies [26], demonstrate that extracting just a single term out of Green's function does not guarantee the smoothness of the remaining part of the integrant, in order to be accurately computed with a low order numerical integration rule. A more robust elimination of the singularity requires the extraction of a second term. Here we follow the latter approach, to take advantage of the low order of numerical integration given the large dimension of the problem.

5. The singular integrals

Recall that $\mathbf{Q}_n(\mathbf{r}')$ are the basis functions for the surface magnetic field, through the surface equivalence principle it follows that

$$\hat{\mathbf{n}}' \times \mathbf{Q}_n(\mathbf{r}') = \mathbf{J_s}(\mathbf{r}'), \quad \hat{\mathbf{n}} \times \mathbf{Q}_m(\mathbf{r}) = \mathbf{J_s}(\mathbf{r})$$

where $\mathbf{J_s}(\mathbf{r}')$ the surface current density at the source-integration point $\mathbf{r}'$. As a first common approach for all the singular integrals to be tackled in this section we begin by introducing a basis for the electric current density on the surface of the domain, and consequently replace the tangential component of the magnetic field or its test function with the current density vector. In this context we can write the electric current density on the surface of the domain as a linear combination of the vector basis functions $\mathbf{f}_n$ as

$$\mathbf{J_s}(\mathbf{r}) = \sum_{n=1}^{ns} \alpha_n \mathbf{f}_n(\mathbf{r})$$

where the function $\mathbf{f}_n(\mathbf{r})$ is defined on the n'th boundary edge and has its support over the two triangular patches sharing the edge,

$$\mathbf{f}_n(\mathbf{r}) = \begin{cases} \frac{l_n \boldsymbol{\rho}_n^+(\mathbf{r})}{2A_n^+} & \mathbf{r} \in T_n^+ \\ \frac{l_n \boldsymbol{\rho}_n^-(\mathbf{r})}{2A_n^-} & \mathbf{r} \in T_n^- \\ 0 & elsewhere \end{cases} \tag{5.0.6}$$

where

$$\boldsymbol{\rho}_n^+(\mathbf{r}) = (\mathbf{r} - n), \quad \boldsymbol{\rho}_n^-(\mathbf{r}) = (n - \mathbf{r})$$

with n the free vertex of the triangle, i.e. the one opposite edge n, l_n the length of the edge, and $A_n^{\pm}$ the areas of the two triangles. The above basis functions illustrated in figure 5 are also known as RWG functions due to the authors who have suggested them in 1984. The same figure indicates also that the RWG functions have span over pairs of surface triangles, hence we shall quote S_n the support of the function $f_n(\mathbf{r})$, referring to the pair of patches sharing the edge n, i.e. $S_n = \{T_n^+, T_n^-\}$.

In the following we argue the case that the singularity in the integrals involving the Green's function or its derivatives is evoked when the field point; and therefore the field triangle, is *close* to the source triangle S'. For consistency in the following we define the term 'closeness'. Two triangular surface elements are said to be close if they share one or more nodes (vertices in simplex elements). Alternatively, as in Hodges et al. it is possible to define manually the closeness by setting an appropriate upper bound on the distance measured from the centroid of the source triangle to the observation point.

5.1. The singular integral $\mathbf{D^1}$.

The simplified expression for the surface integral $\mathbf{D^1}$, involving the product of the scalar Green's function with an RWG function indicates that it is $(1/R)$ singular when the boundary surfaces $\{S, S'\}$ are located close. Here we present the procedure for extracting its singularity. The process is rather similar to that we shall apply for the singular integral $\mathbf{D^2}$ albeit that is $(1/R^2)$ singular as it contains the gradient of the Green's function. We begin demonstrating the technique with $\mathbf{D^1}$ as its simpler form will enhance the clarity

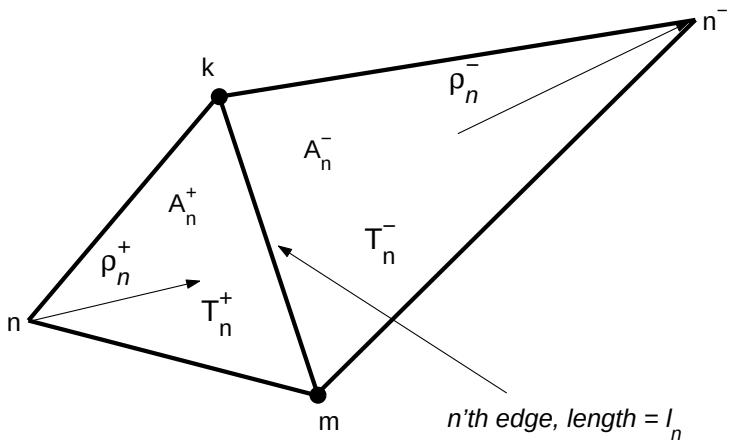

FIGURE 5. The basis of Rao-Wilton-Glisson functions used for the expansion of the surface equivalence currents in the MFIE. The vertex n on the facet T_n^+ is the free vertex of the patch located opposite the n'th edge.

of the derivations. Recall that the integral we seek to evaluate has the form

$$\mathbf{D^1}_{m,n} = jk_0 Y_0 \oint_S \big(\hat{\mathbf{n}} \times \mathbf{L}_m(\mathbf{r})\big) \cdot \hat{\mathbf{n}}(\mathbf{r}) \times \Big(\oint_{S'} G(\mathbf{r},\mathbf{r}') \, \big(\hat{\mathbf{n}}(\mathbf{r}') \times \mathbf{L}_n(\mathbf{r}')\big) \, \mathrm{ds}' \Big) \, \mathrm{ds}$$

and it becomes singular for $\mathbf{r}$ in the support of $\mathbf{L}_n$. As pointed out in Yla-Oijala et al., Eibert et al., we begin by extracting two terms from the kernel of the Green's function, transforming the above integral into a sum of integrals

$$\begin{aligned} \mathbf{D^1}_{m,n} = jk_0 Y_0 \oint_S \mathbf{f}_m(\mathbf{r}) \cdot \hat{\mathbf{n}}(\mathbf{r}) \times \Big[& \oint_{S'} \Big(\frac{e^{-jk_0 R} - 1}{4\pi R} + \frac{k_0^2 R}{8\pi} \Big) \mathbf{f}_n(\mathbf{r}') \, \mathrm{ds}' \\ & + \frac{1}{4\pi} \oint_{S'} R^{-1} \, \mathbf{f}_n(\mathbf{r}') \, \mathrm{ds}' \\ & - \frac{k_0^2}{8\pi} \oint_{S'} R \, \mathbf{f}_n(\mathbf{r}') \, \mathrm{ds}' \Big] \, \mathrm{ds} \end{aligned} \tag{5.1.1}$$

where $\mathbf{f}_n(\mathbf{r}')$ is numerically equivalent to $\big(\hat{\mathbf{n}}(\mathbf{r}') \times \mathbf{L}_n(\mathbf{r}')\big)$ and their definitions are given in (5.0.6). Also, notice that the singular integrants above are of the form $R^k \, \mathbf{f}_n(\mathbf{r}')$ for $k = 1$ and $k = -1$, while the remaining part of the integrant is a sufficiently smooth function with

$$\lim_{R \to 0} \Big\{ \frac{e^{-jk_0 R} - 1}{4\pi R} + \frac{k_0^2 R}{8\pi} \Big\} = -j \frac{k_0}{4\pi} \tag{5.1.2}$$

For the singular integrals the common practice is to apply Gauss integral theorems so that to transform the integration from the surface of the triangular patch, to a sum of line integrals over the edges of the patch, e.g.

$$\oint_S R^n \, \mathrm{ds} = f\left(\sum_{i=1}^{3} \oint_{\partial_i S} R^n \, \mathrm{dl} \right) \tag{5.1.3}$$

Provided the integrant in the first term of (5.1.1) is continuously differentiable functions, (at least C^2), this is evaluated numerically, while the singular integrals will be computed using analytical expressions. In general terms our strategy is to express the pertinent singular integrals in terms of

$$\oint_{S'} \frac{1}{R}\,\mathrm{ds}' \qquad \text{and} \qquad \oint_{S'} R\,\mathrm{ds}'$$

for which we have analytic expressions based on the geometry of the surface elements, e.g. triangles, from [40], [14], [16] and [26]. According to these,

$$\begin{aligned}\oint_{S'} \frac{1}{R}\,\mathrm{ds}' &= \sum_{i=1}^{3} t_i^0 \oint_{\partial_i S'} \frac{1}{R}\,\mathrm{dl}' \qquad\qquad \text{for} \quad w_0 = 0 \\ &= -w_0\Big(w_0 \oint_{S'} \frac{1}{R^3}\,\mathrm{ds}'\Big) + \sum_{i=1}^{3} t_i^0 \oint_{\partial_i S'} \frac{1}{R}\,\mathrm{dl}' \quad \text{for} \quad w_0 \neq 0\end{aligned} \tag{5.1.4}$$

where

$$\oint_{\partial_i S'} \frac{1}{R}\,\mathrm{dl}' = \ln\Big(\frac{R_i^+ + s_i^+}{R_i^- + s_i^-}\Big) \tag{5.1.5}$$

and

$$w_0 \oint_{S'} \frac{1}{R^3}\,\mathrm{ds}' = \mathrm{sgn}(w_0)\,\beta \tag{5.1.6}$$

with

$$\beta = \sum_{i=1}^{3}\Big(\arctan\Big(\frac{t_i^0 s_i^+}{(R_i^0)^2 + |w_0| R_i^+}\Big) - \arctan\Big(\frac{t_i^0 s_i^-}{(R_i^0)^2 + |w_0| R_i^-}\Big)\Big) \tag{5.1.7}$$

Similarly,

$$\begin{aligned}\oint_{S'} R\,\mathrm{ds}' &= \frac{1}{3}\sum_{i=1}^{3} t_i^0 \oint_{\partial_i S'} R\,\mathrm{dl}' \qquad\qquad \text{for} \quad w_0 = 0 \\ &= \frac{1}{3}\Big(w_0^2 \oint_{S'} \frac{1}{R}\,\mathrm{ds}'\Big) + \sum_{i=1}^{3} t_i^0 \oint_{\partial_i S'} R\,\mathrm{dl}' \quad \text{for} \quad w_0 \neq 0\end{aligned} \tag{5.1.8}$$

where

$$\oint_{\partial_i S'} R\,\mathrm{dl}' = \frac{1}{2}\Big(s_i^+ R_i^+ - s_i^- R_i^- + (R_i^0)^2 \cdot \oint_{\partial_i S'} \frac{1}{R}\,\mathrm{dl}'\Big) \tag{5.1.9}$$

The integral $\mathbf{D^1}$ involves the integral of the product of the Green's function with an RWG function. As above we proceed by extracting two singular terms out of Green's function, while we focus our attention to the $(1/R)$ singularity case in which S and S' are close. For clarity also allow, $\mathbf{f}_m(\mathbf{r})$ and $\mathbf{f}_n(\mathbf{r}')$ to be the two RWG functions involved in the integral belonging to the m'th edge of S and n'th edge of S' respectively. According to this notation the pertinent integral is

$$\begin{aligned}\mathbf{D^1}_{m,n} = jk_0 Y_0 \oint_S \mathbf{f}_m(\mathbf{r}) \cdot \hat{\mathbf{n}}(\mathbf{r}) \times \oint_{S'} \Big[&\frac{2(e^{-jk_0 R} - 1) + k_0^2 R^2}{8\pi R} \\ &+ \frac{1}{4\pi R} - \frac{k_0^2 R}{8\pi}\Big]\mathbf{f}_n(\mathbf{r}')\,\mathrm{ds}'\,\mathrm{ds}\end{aligned} \tag{5.1.10}$$

Substituting the definitions of the basis and test functions

$$\mathbf{f}_m(\mathbf{r}) = \frac{l_m}{2A_S}(\mathbf{r} - m), \qquad \mathbf{f}_n(\mathbf{r}') = \frac{l_n}{2A_{S'}}(\mathbf{r}' - n)$$

we get

(5.1.11)

$$\mathbf{D^1}_{m,n} = jk_0Y_0\frac{l_m l_n}{4A_SA_{S'}}\Big[\oint_S(\mathbf{r}-m)\cdot\hat{\mathbf{n}}(\mathbf{r})\times\Big(\oint_{S'}(\mathbf{r}'-n)\frac{2(e^{-jk_0R}-1)+k_0^2R^2}{8\pi R}\,\mathrm{ds}' + \frac{1}{4\pi}\oint_{S'}(\mathbf{r}'-n)\frac{1}{R}\,\mathrm{ds}' - \frac{k_0^2}{8\pi}\oint_{S'}(\mathbf{r}'-n)R\,\mathrm{ds}'\Big)\mathrm{ds}\Big]$$

where the vectors $(\mathbf{r} - m)$ and $(\mathbf{r}' - n)$ are defined from the free vertices m, and n, toward $\mathbf{r}$ and $\mathbf{r}'$ respectively. As before, the first term is now smooth enough to undergo a low order numerical integration, while the remaining two involving the integral of R and R^{-1} will be evaluated via analytic formulae. Using the results from the previous section (on $\mathbf{D^2}$), for the pertinent integrals in $\mathbf{D^1}$ we have

$$\oint_{S'}(\mathbf{r}'-n)\frac{1}{R}\,\mathrm{ds}' = \sum_{i=1}^{3}\hat{\mathbf{m}}_i\cdot\oint_{\partial_i S'}R\,\mathrm{dl}' + (\boldsymbol{\rho}-n)\oint_{S'}\frac{1}{R}\,\mathrm{ds}' \tag{5.1.12}$$

with $\boldsymbol{\rho} = \mathbf{r} - w_0\hat{\mathbf{n}}$, and

$$\oint_{S'}(\mathbf{r}'-n)R\,\mathrm{ds}' = \frac{1}{3}\sum_{i=1}^{3}\hat{\mathbf{m}}_i\oint_{\partial_i S'}R^3\,\mathrm{dl}' + (\boldsymbol{\rho}-n)\oint_{S'}R\,\mathrm{ds}' \tag{5.1.13}$$

where

$$\oint_{\partial_i S'}R^3\,\mathrm{dl} = \frac{1}{4}\Big(s_i^+(R_i^+)^3 - s_i^-(R_i^-)^3 + 3(R_i^0)^2\cdot\oint_{\partial_i S'}R\,\mathrm{dl}'\Big) \tag{5.1.14}$$

5.2. **The singular integral $\mathbf{D^2}$.** The singular integral $\mathbf{D^2}$ is given by

$$\mathbf{D^2}_{m,n} = -j\frac{Y_0}{k_0}\oint_S\big(\hat{\mathbf{n}}\times\mathbf{L}_m(\mathbf{r})\big)\cdot\hat{\mathbf{n}}(\mathbf{r})\times \Big(\nabla'\cdot\big(\hat{\mathbf{n}}(\mathbf{r}')\times\mathbf{L}_n(\mathbf{r}')\big)\oint_{S'}\nabla'G(\mathbf{r},\mathbf{r}')\,\mathrm{ds}'\Big)\,\mathrm{ds}$$

where the inner integral over the source triangle is obviously $1/R^2$ singular due to the gradient of the Green's function. In response, following the singularity extraction approach as before we write the scalar Green's function as

$$G(\mathbf{r},\mathbf{r}') = \Big(G(\mathbf{r},\mathbf{r}') - \frac{1}{4\pi R} + \frac{k_0^2}{8\pi}R\Big) + \frac{1}{4\pi R} - \frac{k_0^2}{8\pi}R \tag{5.2.1}$$

Taking the gradient with respect to the source variable on both sides of the above and integrate over the source element yields

$$\oint_{S'}\nabla'G(\mathbf{r},\mathbf{r}')\,\mathrm{ds}' = \oint_{S'}\nabla'q(R)\,\mathrm{ds}' + \frac{1}{4\pi}\oint_{S'}\nabla'\frac{1}{R}\,\mathrm{ds}' - \frac{k_0^2}{8\pi}\oint_{S'}\nabla'R\,\mathrm{ds}' \tag{5.2.2}$$

where $q(R)$ is the smooth bracketed function above with gradient

$$\nabla'q(R) = \Big(\frac{2e^{-jk_0R}(jk_0R+1) - k_0^2R^2 - 2}{8\pi R^3}\Big)\mathbf{R} \tag{5.2.3}$$

and limit

$$\lim_{R\to 0} \nabla' q(R) = -j\frac{k^3}{12\pi}\mathbf{R} \tag{5.2.4}$$

Whilst the integral of $\nabla' q(R)$ can be computed numerically using Gaussian quadrature rules, the two singular integrals can be computed using analytically extracted formulae. See [14] and [26]. More specifically,

$$\oint_{S'} \nabla' R \, \mathrm{ds}' = \sum_{i=1}^{3} \hat{\mathbf{m}}_i \oint_{\partial_i S'} R \, \mathrm{dl}' - \hat{\mathbf{n}}(\mathbf{r}') \cdot w_0 \oint_{S'} \frac{1}{R} \, \mathrm{ds}' \tag{5.2.5}$$

and

$$\oint_{S'} \nabla' \frac{1}{R} \, \mathrm{ds}' = \sum_{i=1}^{3} \hat{\mathbf{m}}_i \oint_{\partial_i S'} \frac{1}{R} \, \mathrm{dl}' + \hat{\mathbf{n}}(\mathbf{r}') \cdot w_0 \oint_{S'} \frac{1}{R^3} \, \mathrm{ds}' \tag{5.2.6}$$

5.3. **The singular integral $\mathbf{C^2}$.** Let us begin with the first integral involving the dyadic Green's function in free-space

$$\mathbf{C^2}_{m,n} = -\oint_S (\hat{\mathbf{n}} \times \mathbf{L}_m(\mathbf{r})) \cdot \Big(\hat{\mathbf{n}}(\mathbf{r}) \times \oint_{S'} \nabla' G(\mathbf{r}, \mathbf{r}') \times \big(\hat{\mathbf{n}}(\mathbf{r}') \times \mathbf{L}_n(\mathbf{r}') \big) \, \mathrm{ds}' \Big) \, \mathrm{ds}$$

Let us focus our attention for a while on the second integral in the above which describes the scattered magnetic field. For a pair of triangles $\{S, S'\}$, which are close together but *not* on the same plane, this integral contains a $(1/R^2)$ singularity, however, if the two triangles are on the same plane or overlapping the value of the integral vanishes. To verify this, let p be the plane of S and S'. Now the gradient of the green's function will be a vector tangential on p and so is $\hat{\mathbf{n}}(\mathbf{r}') \times \mathbf{L}_n(\mathbf{r}')$, in fact in this case $\hat{\mathbf{n}}(\mathbf{r}') = \hat{\mathbf{n}}(\mathbf{r})$. This implies that the cross product of the inner integral (over S') is a vector normal to p. In effect, the inner integrant is orthogonal to the tangential of the shape function $\mathbf{L}_m$, and hence their dot product is zero. Now, for clarity we isolate the inner integral as

$$H^n(\mathbf{r}) = \oint_{S'}^{c} \nabla' G(\mathbf{r}, \mathbf{r}') \times (\hat{\mathbf{n}}' \times L_n(\mathbf{r}')) \, \mathrm{ds}' \tag{5.3.1}$$

Plugging in the formula for the gradient of the scalar Green's function (4.0.8) with respect to the primed coordinates yields

$$H^n(\mathbf{r}) = \frac{1}{4\pi} \oint_{S'}^{c} \Big(jk_0 + \frac{1}{R} \Big) \hat{\mathbf{R}} \times {\mathbf{J_s}}^n(\mathbf{r}') \frac{e^{-jk_0 R}}{R} \, \mathrm{ds}'$$

and therefore the overall integral is now

$$\mathbf{C^2}_{m,n} = -\frac{1}{4\pi} \oint_S \mathbf{f}_m(\mathbf{r}) \cdot \Big[\hat{\mathbf{n}}(\mathbf{r}) \times \oint_{S'} \Big(jk_0 + \frac{1}{R} \Big) \hat{\mathbf{R}} \times {\mathbf{J_s}}^n(\mathbf{r}') \frac{e^{-jk_0 R}}{R} \, \mathrm{ds}' \Big] \, \mathrm{ds}$$

We shall now consider the evaluation of the integral in the situations were the RWG functions involved have supports which are close to each other but these are defined on edges whose parent triangles are on different planes. If $\boldsymbol{\rho}'_n = \boldsymbol{\rho}_n(\mathbf{r}') = (\mathbf{r}' - n)$, then substituting into the formula for $H^n(\mathbf{r})$ gives

$$H^n(\mathbf{r}) = \frac{l_n}{8\pi A_{S'}} \oint_{S'} \Big(jk_0 + \frac{1}{R} \Big) \hat{\mathbf{R}} \times \boldsymbol{\rho}'_n \frac{e^{-jk_0 R}}{R} \, \mathrm{ds}'$$

The vector $\mathbf{R}$ can be expressed in terms of the source related vector $\boldsymbol{\rho}'_n$ and the observation related vector $\mathbf{R}_n$ which is constant with respect to the variable of integration, so the cross product in the above can be further developed to

$$\hat{\mathbf{R}} \times \boldsymbol{\rho}'_n = \frac{\mathbf{R}}{R} \times \boldsymbol{\rho}'_n = \frac{\mathbf{R}_n - \boldsymbol{\rho}'_n}{R} \times \boldsymbol{\rho}'_n = \frac{1}{R}(\mathbf{R}_n \times \boldsymbol{\rho}'_n) \tag{5.3.2}$$

yielding,

$$H^n(\mathbf{r}) = \frac{l_n}{8\pi A_{S'}} \mathbf{R}_n \times \oint_{S'} \boldsymbol{\rho}'_n \frac{(jk_0R+1)e^{-jk_0R}}{R^3}\, \mathrm{ds}' \tag{5.3.3}$$

where $\mathbf{R}_n$ is the vector from the n'th vertex in the source face to the observation point $\mathbf{r}$. This substitution effectively removes the cross product outside the integral, hence simplifying its computation. Following the singularity extraction approach the above can be expanded as

$$\begin{aligned} H^n(\mathbf{r}) = \frac{l_n}{8\pi A_{S'}} \mathbf{R}_n \times \Bigg[& \oint_{S'} \boldsymbol{\rho}'_n \frac{(jk_0R+1)e^{-jk_0R} - (1+\frac{1}{2}k_0^2R^2)}{R^3}\, \mathrm{ds}' \\ & + \oint_{S'} \frac{\boldsymbol{\rho}'_n}{R^3}\, \mathrm{ds}' + \frac{k_0^2}{2} \oint_{S'} \frac{\boldsymbol{\rho}'_n}{R}\, \mathrm{ds}' \Bigg] \end{aligned} \tag{5.3.4}$$

where the pertinent singular integrals are of the form

$$\oint_{S'} (\mathbf{r}' - n) \frac{1}{R^3}\, \mathrm{ds}' \quad \text{and} \quad \oint_{S'} (\mathbf{r}' - n) \frac{1}{R}\, \mathrm{ds}' \tag{5.3.5}$$

while the remaining integrant multiplying $\boldsymbol{\rho}'_n$ is now smooth enough with

$$\lim_{R\to 0} \Big\{ \frac{(jk_0R+1)e^{-jk_0R} - (1+\frac{1}{2}k_0^2R^2)}{R^3} \Big\} = -\frac{1}{3} jk_0^3 \tag{5.3.6}$$

The formula for calculating the integral on the right has already been provided as the same integral appears also in the construction of $\mathbf{D^2}$, while for the one in the left we have

$$\oint_{S'} (\mathbf{r}' - n) \frac{1}{R^3}\, \mathrm{ds}' = -\sum_{i=1}^{3} \hat{\mathbf{m}}_i \ln\Big(\frac{R_i^+ + s_i^+}{R_i^- + s_i^-} \Big) + (\boldsymbol{\rho} - n) \oint_{S'} \frac{1}{R^3}\, \mathrm{ds}' \tag{5.3.7}$$

where for $w_0 \neq 0$

$$\oint_{S'} \frac{1}{R^3}\, \mathrm{ds}' = \frac{\mathrm{sgn}(w_0)}{w_0} \beta \tag{5.3.8}$$

In effect, the singular entries of the integral $\mathbf{C^2}$ are given by

$$\begin{aligned} \mathbf{C^2}_{m,n} = & -\frac{l_m l_n}{16\pi A_S A_{S'}} \oint_S (\mathbf{r} - m) \cdot \hat{\mathbf{n}}(\mathbf{r}) \times \\ & \Bigg\{ (\mathbf{r} - n) \times \Big[\oint_{S'} (\mathbf{r}' - n) \frac{(jk_0R+1)e^{-jk_0R} - (1+\frac{1}{2}k_0^2R^2)}{R^3}\, \mathrm{ds}' \\ & + \oint_{S'} (\mathbf{r}' - n) \frac{1}{R^3}\, \mathrm{ds}' + \frac{k_0^2}{2} \oint_{S'} (\mathbf{r}' - n) \frac{1}{R}\, \mathrm{ds}' \Big] \Bigg\} \end{aligned} \tag{5.3.9}$$

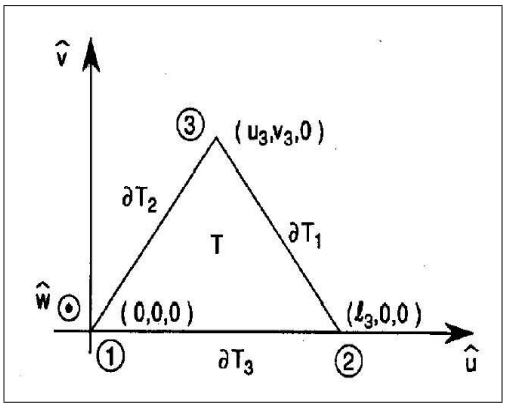

(a)

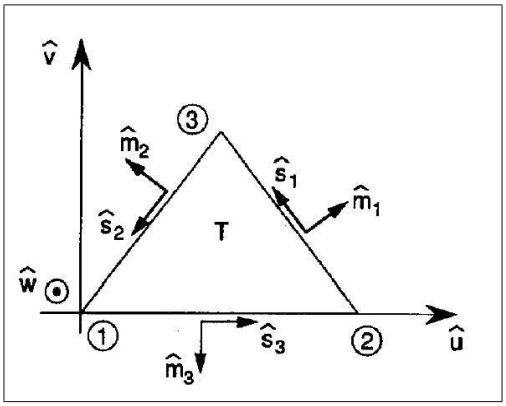

(b)

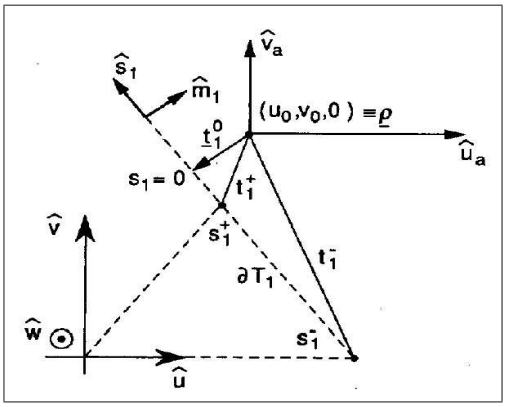

(c)

FIGURE 6. The surface triangular patch in the local set of coordinates $\mathcal{L}$ used in the analytical integration. Figures extracted from [14].

Variable	Description
$\hat{\mathbf{n}}$	Unit normal on S.
$\mathbf{r}$	The observation point in S.
$\mathbf{r}'$	The integration point in S.
O	Origin point. (e.g. geometric center of S).
O'	Projection of the origin to S.
w_0	Distance from $\mathbf{r}$ to S, $w_0 = (\mathbf{r} - \hat{\mathbf{n}})v$.
R	Vector from $\mathbf{r}$ to $\mathbf{r}'$.
$\boldsymbol{\rho}$	Vector from O' to $\mathbf{r}$, $\boldsymbol{\rho} = (\mathbf{r} - w_0\hat{\mathbf{n}})$
ρ'	Vector from O' to $\mathbf{r}'$.
ρ_n	Vector from O' to the vertex n.
ρ'_n	Vector from vertex n to $\mathbf{r}'$.
R_n	Vector from vertex n to $\mathbf{r}$.
$\hat{\mathbf{s}}_n$	Unit vector on edge n in the direction of T_n.
$\hat{\mathbf{m}}_n$	Unit normal on edge n in the plane of S.
t_n^0	Distance from ρ to the edge n.
$\hat{t}_n^0$	Unit vector in the direction of t_n^0.
s_n^-	Distance from t_n^0 to the beginning of the edge n.
s_n^+	Distance from t_n^0 to the end of the edge n.
t_n^+	The distance $\sqrt{(t_n^0)^2 + (s_n^+)^2}$.
t_n^-	The distance $\sqrt{(t_n^0)^2 + (s_n^-)^2}$.
R_n^0	The distance $\sqrt{(t_n^0)^2 + w_0^2}$.
R_n^+	The distance $\sqrt{(t_n^+)^2 + w_0^2}$.
R_n^-	The distance $\sqrt{(t_n^-)^2 + w_0^2}$.

TABLE 2. The parameters used in the computation of the singular integrals on the triangular surface patches S.

5.4. **Numerical evaluation of singular integrals.** For the numerical evaluation of the singular integrals we follow the convention that the n'th edge of any surface triangle, where $n = 1 : 3$, is the one positioned across the n'th vertex of the same surface element, the so called free vertex. This reflects the sequence in the elements of the rows of `srf` and `srfedg` matrices, which denote the connectivity of the surface triangular patches in vertices and edges respectively. If P_n, denote the column coordinate vectors for the vertices of the k'th triangle, the edge unit (tangential) vectors are

$$\hat{\mathbf{s}}_1 = (P_3 - P_2)/l_1, \quad \hat{\mathbf{s}}_2 = (P_1 - P_3)/l_2, \quad \hat{\mathbf{s}}_3 = (P_2 - P_1)/l_3 \tag{5.4.1}$$

where the length l_n of the n'th edge of the k'th surface is obtained as $l_n =$ `deg(srfedg(k,n))`. The above should satisfy $\sum_{i=1}^{3} l_i \hat{\mathbf{s}}_i = 0$. Next, the unit outward normal vectors on each of the edges can be computed using

$$\hat{\mathbf{m}}_n = \hat{\mathbf{s}}_n \times \hat{\mathbf{n}} \tag{5.4.2}$$

and these satisfy $\sum_{i=1}^{3} l_i \hat{\mathbf{m}}_i = 0$. Now, in the local coordinates $(\hat{u}, \hat{v}, \hat{w})$, the unit vectors on the local axes are

$$\hat{u} = (P_2 - P_1)/l_3, \quad \hat{v} = \hat{\mathbf{n}} \times \hat{u}, \quad \hat{w} = \hat{\mathbf{n}} \tag{5.4.3}$$

with

$$\begin{bmatrix} \hat{u}\cdot\hat{\mathbf{s}}_i \\ \hat{v}\cdot\hat{\mathbf{s}}_i \end{bmatrix} = \begin{bmatrix} -\hat{v}\cdot\hat{\mathbf{m}}_i \\ \hat{u}\cdot\hat{\mathbf{m}}_i \end{bmatrix}$$

If the patch in the local coordinate system lies on the $(\hat{u},\hat{v})$ plane with two of its vertices at $(0,0,0)$ and $(l_3,0,0)$, then the coordinates of the third vertex $(\hat{u}_3,\hat{v}_3,0)$ and the observation point $\mathbf{r}(x,y,z)$ are given by

$$\hat{u}_3 = (P_3-P_1)\cdot\hat{u}, \quad \hat{v}_3 = \|\hat{\mathbf{n}}\|/l_3 \quad \text{and} \quad \begin{bmatrix} u_0 \\ v_0 \\ w_0 \end{bmatrix} = \begin{bmatrix} \hat{u} \\ \hat{v} \\ \hat{w} \end{bmatrix} \cdot (\mathbf{r}-P_1) \tag{5.4.4}$$

where w_0 is the distance from the observation point to the plane of the integration S', measured positively in the direction of $\hat{\mathbf{n}}$. The cross section of the line $\hat{w}=w_0$ with $S'(\hat{u},\hat{v},0)$, yields the coordinates of the projected observation point $\rho(u_0,v_0,0)$ for which we can compute

$$\begin{aligned} s_1^- &= -\frac{(l_3-u_0)(l_3-u_3)+v_0v_3}{l_1} \\ s_1^+ &= \frac{(u_3-u_0)(u_3-l_3)+v_3(v_3-v_0)}{l_1} = s_1^- + l_1 \\ s_2^- &= -\frac{u_3(u_3-u_0)+v_3(v_3-v_0)}{l_2} \\ s_2^+ &= \frac{u_0u_3+v_0v_3}{l_2} = s_2^- + l_2 \\ s_3^- &= -u_0, \quad s_3^+ = l_3-u_0 \end{aligned} \tag{5.4.5}$$

as well as the quantities

$$\begin{aligned} &t_1^0 = \frac{v_0(u_3-l_3)+v_3(l_3-u_0)}{l_1}, \quad t_2^0 = \frac{u_0v_3-v_0u_3}{l_2}, \quad t_3^0 = v_0 \\ &t_1^- = \sqrt{(l_3-u_0)^2+v_0^2}, \quad t_1^+ = \sqrt{(u_3-u_0)^2+(v_3-v_0)^2}, \quad t_2^- = t_1^+ \\ &t_2^+ = \sqrt{u_0^2+v_0^2}, \quad t_3^- = t_2^+, \quad t_3^+ = t_1^- \end{aligned} \tag{5.4.6}$$

The distance from the observation point to each of the edges of S' is

$$R_1^0 = \sqrt{(t_1^0)^2+w_0^2},\ R_2^0 = \sqrt{(t_2^0)^2+w_0^2},\ R_3^0 = \sqrt{(t_3^0)^2+w_0^2} \tag{5.4.7}$$

while if $\mathbf{r}$ is on the plane of S', the distance w_0 is zero and $R_i^0 = t_i^0$. Similarly, R_i^+ and R_i^- are the distances from the observation point towards the beginning and end of the i'th edge in S', so that

$$R_1^\pm = \sqrt{(t_1^\pm)^2+w_0^2},\ R_2^\pm = \sqrt{(t_2^\pm)^2+w_0^2},\ R_3^\pm = \sqrt{(t_3^\pm)^2+w_0^2} \tag{5.4.8}$$

6. Excitation conditions: The physical experiment

The external excitation conditions we wish to apply reflect those of the physical experiment described in [25]. In brief, a monochromatic and arbitrarily polarization impinges the outer surface of the liquid crystal at the part of the boundary Γ_1, and propagates in the arbitrary direction set by the pair of azimuthal incidence angles

(ϕ^i, θ^i). Here we assume the the incident signal is a *plane wave*. In this situation, the exterior excitation term ψ_i^{ext} is given by

$$\psi_i^{ext} = -jk_0 Z_0 \oint_S \mathbf{T}_i \cdot \hat{\mathbf{n}} \times (\mathbf{H}^i + \mathbf{H}^r)\, \mathrm{ds} \tag{6.0.9}$$

where $\mathbf{T}_i = \hat{\mathbf{n}} \times \mathbf{L}_i$ are the test functions associated with $\mathbf{H}^{ext}$. For the plane wave, the incidence magnetic field is given by

$$\mathbf{H}^i(\mathbf{r}) = Y_0\big(\hat{\mathbf{k}}^i \times \mathbf{E}^i(\mathbf{r})\big) \tag{6.0.10a}$$

where

$$\mathbf{E}^i(\mathbf{r}) = \hat{\mathbf{p}}^i \exp\big(-jk_0(\hat{\mathbf{k}}^i \cdot \mathbf{r})\big) \tag{6.0.10b}$$

where $\hat{\mathbf{p}}^i$ is the polarization and $\hat{\mathbf{k}}^i$ is the direction of the incident field given as

$$\hat{\mathbf{k}}^i = -\begin{bmatrix}\cos\phi^i \sin\theta^i & \sin\phi^i \sin\theta^i & \cos\theta^i\end{bmatrix}^T \tag{6.0.10c}$$

where (ϕ^i, θ^i) denote the polarization angles of the incident plane wave. In a similar manner for the reflected magnetic component of the incident wave we have

$$\mathbf{H}^r(\mathbf{r}) = Y_0\big(\hat{\mathbf{k}}^r \times \mathbf{E}^r(\mathbf{r})\big) \tag{6.0.10d}$$

where

$$\mathbf{E}^r(\mathbf{r}) = \hat{\mathbf{p}}^r \exp\big(-jk_0(\hat{\mathbf{k}}^r \cdot \mathbf{r})\big) \tag{6.0.10e}$$

with

$$\hat{\mathbf{k}}^r = -\begin{bmatrix}\cos\phi^i \sin\theta^i & \sin\phi^i \sin\theta^i & -\cos\theta^i\end{bmatrix}^T \tag{6.0.10f}$$

For example, if the incident field is $\hat{\mathbf{p}}^i = \begin{bmatrix}\mathbf{p}^{ix} & \mathbf{p}^{iy} & \mathbf{p}^{iz}\end{bmatrix}^T$ and the direction of propagation is $\hat{\mathbf{k}}^i = \begin{bmatrix}\mathbf{k}^{ix} & \mathbf{k}^{iy} & \mathbf{k}^{iz}\end{bmatrix}^T$ then at a point $\mathbf{r}(x, y, z) \in \Gamma_1$, such that $\hat{\mathbf{k}}^i \cdot \mathbf{r} = \alpha$ and $\mathbf{r} \in \Gamma_1$, the incident electric field is evaluated as

$$\mathbf{E}^i(\mathbf{r}) = \begin{bmatrix}\mathbf{p}^{ix}\exp(-jk_0\alpha) & \mathbf{p}^{iy}\exp(-jk_0\alpha) & \mathbf{p}^{iz}\exp(-jk_0\alpha)\end{bmatrix}^T$$

subsequently yielding $\mathbf{H}^i = Y_0(\hat{\mathbf{k}}^i \times \mathbf{E}^i)$. A similar procedure is repeated for the reflected component of the plane wave.

7. Forward computations

On a non empty subset of the boundary $\Gamma_1 \subset \partial\Omega$ we apply excitation by means of an input polarized plane wave ψ^{ext}. For a fixed set of interior electrical parameters this leads to a Neumann to Dirichlet operator $\Lambda_{\boldsymbol{\epsilon}} : \mathbf{Y} \to \mathbf{Z}$ of the form

$$\Lambda_{\boldsymbol{\epsilon}} \triangleq \hat{\mathbf{n}}(\mathbf{r}) \times \mathbf{H}(\mathbf{r}) \rightarrowtail \hat{\mathbf{n}}(\mathbf{r}) \times \mathbf{E}(\mathbf{r}) \qquad \mathbf{r} \in \partial\Omega \tag{7.0.11}$$

This smooth injective operator maps uniquely the tangential components of the magnetic field to their corresponding tangential components of the electric field at the surface of the domain. Fixing the Neumann conditions we can proceed to formulate the nonlinear forward operator $\Phi : \mathbf{X} \to \mathbf{Z}$

$$\Phi \triangleq \boldsymbol{\epsilon}(\mathbf{r})\big|_{\mathbf{r}\in\Omega} \mapsto \hat{\mathbf{n}}(\mathbf{r}) \times \mathbf{E}(\mathbf{r})\big|_{\mathbf{r}\in\Gamma_2} \tag{7.0.12}$$

where $\Gamma_2 \subset \partial\Omega$, $\Gamma_2 \neq \Gamma_1$ is the part of the boundary where the polarization measurement is gathered. Operator Φ is nonlinear in $\boldsymbol{\epsilon}$, is non-injective and (at

least) twice continuously differentiable in the domain of interest, $\Phi \in C^2(\Omega)$. Let us define the Maxwell operator $M_{(\boldsymbol{\epsilon})} : \mathbf{X} \to \mathbb{L}^2_{curl}(\Omega)^3$

$$M_{(\boldsymbol{\epsilon})} = \begin{bmatrix} \mathbf{A} & \mathbf{B} \\ \mathbf{D} & \mathbf{C} \end{bmatrix} \tag{7.0.13}$$

and the *direct forward problem* as

$$M_{(\boldsymbol{\epsilon})} \begin{bmatrix} E \\ H_s \end{bmatrix} = \begin{bmatrix} 0 \\ \psi^{ext} \end{bmatrix} \tag{7.0.14}$$

where E and H_s are the tangential components of the electric field in the closure of the domain and that of the magnetic field at the boundary of the domain respectively. Moreover, allow a measurements operator $P : \mathbb{L}^2_{curl}(\Omega)^3 \to \mathbf{Z}$ which extracts a set of boundary electric field measurements at the positions of the detectors given a distribution of electric field

$$P(\mathbf{E}) = \zeta \tag{7.0.15}$$

where $\zeta \in \mathbf{Z}$ is a vector of complex measurements.

7.1. **Linearization.** Once the forward operator has been constructed the next objective is to linearize the problem. Provided that Φ is at least twice continuously differentiable in the spaces $\mathbf{X}$ and $\mathbf{Y}$, taking a strictly feasible point $\delta\boldsymbol{\epsilon} \in \mathbf{X}$ one can compute the Fréchet derivative of Φ, which maps perturbations in the interior permittivity distribution to perturbations in the boundary electric field measurements. Operator $\Phi' : \mathbf{X} \to \mathbf{Y}$ is linear, compact and bounded while in the discrete sense, evaluating Φ' at an admissible point in $\mathbf{X}$ yields an ill-conditioned matrix, the so called Jacobian or sensitivity matrix, with exponentially decaying singular values. The assembling of this matrix is conventionally performed via the perturbation method [28], however here we demonstrate a computationally efficient method for computing the Jacobian based on the adjoint fields technique [8]. For the derivation we consider piecewise constant permittivity tensors on the elements of the model.

Taking the Taylor expansion of Φ and linearizing around an admissible point as in the Newton-Raphson method, neglecting second-order and higher terms we have the *linearized forward problem*

$$\Phi'(\boldsymbol{\epsilon})\ \delta\boldsymbol{\epsilon} = \delta\zeta \tag{7.1.1}$$

where $\Phi'(\boldsymbol{\epsilon})$ is the Fréchet derivative of Φ at $\boldsymbol{\epsilon}$ and $\delta\zeta = P\big(\mathbf{E}(\boldsymbol{\epsilon})\big) - P\big(\mathbf{E}(\boldsymbol{\epsilon} + \delta\boldsymbol{\epsilon})\big)$. Moreover $\delta\zeta$ solves

$$M_{(\boldsymbol{\epsilon})} \begin{bmatrix} \delta\zeta \\ \delta H_s \end{bmatrix} = \begin{bmatrix} \delta\boldsymbol{\epsilon}\, E \\ 0 \end{bmatrix} \tag{7.1.2}$$

In conjunction with the direct problem , if $\overline{X}$ is the complex conjugate of X, we can also define the *adjoint forward problem* as

$$M^*_{(\boldsymbol{\epsilon})} \begin{bmatrix} \mathcal{E} \\ \mathcal{H}_s \end{bmatrix} = \begin{bmatrix} 0 \\ \mathbf{s} \end{bmatrix} \tag{7.1.3}$$

where

$$M^*_{(\boldsymbol{\epsilon})} = \begin{bmatrix} \mathbf{A} & \overline{\mathbf{B}} \\ \overline{\mathbf{D}} & \overline{\mathbf{C}} \end{bmatrix} \tag{7.1.4}$$

and $\mathbf{s}$ is the vector of adjoint sources for the problem [8]. If the k'th measurement is captured at $\Gamma_2 \in \partial\Omega$, then the corresponding adjoint source is that which causes

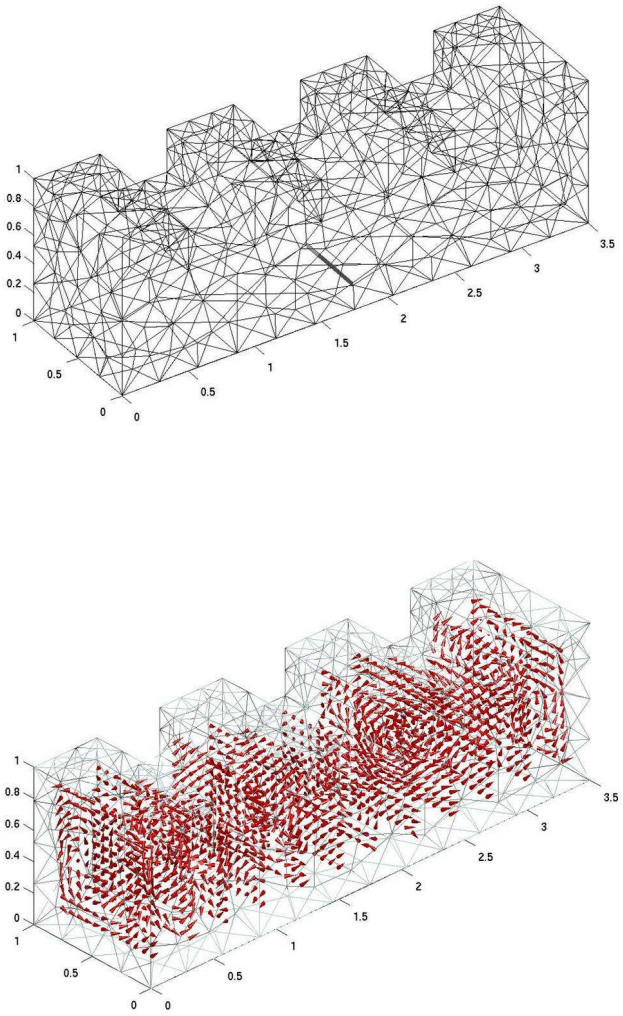

FIGURE 7. At the top: A finite element grid of a liquid crystal cell with gratings, indicating also the point of incident for the incoming laser beam. Below: The computed electric field solution.

a plane wave incident on Γ_2 to propagate backwards into the domain. This sets up the so-called adjoint fields which we denote $\mathcal{E}$ and $\mathcal{H}_s$ associated with the k'th measurement. In a mathematical sense, the back-propagation is expressed via the use of the negative frequency $(-\omega)$ in the definition of the k'th adjoint source $\mathbf{s}^k$ given by

$$\mathbf{s}_i^k = jk_0 Z_0 \oint_{\Gamma_2} \mathbf{F}_i \cdot (\hat{\mathbf{n}} \times \mathbf{H}^{ir})^k \, \mathrm{ds} \tag{7.1.5}$$

To derive the sensitivity of the system which indicates how perturbations on the permittivity $\delta\boldsymbol{\epsilon}$ affect the boundary measurements of the form $\hat{\mathbf{n}}\times\mathbf{E}$ we require the Fréchet derivative of the forward operator. Recall that the weak formulation of the problem assuming homogeneous and isotropic unit magnetic permeability is

$$\int_\Omega (\nabla\times\mathbf{E})(\nabla\times\mathbf{F}) - k_0^2\boldsymbol{\epsilon_r}\mathbf{E}\cdot\mathbf{F}\,\mathrm{d}\Omega = jk_0Z_0\oint_{\partial\Omega}(\hat{\mathbf{n}}\times\mathbf{H})\,\mathbf{F}\,\mathrm{ds} \tag{7.1.6}$$

In the case where $\mathbf{F}=\overline{\mathbf{E}}$ the above becomes

$$\int_\Omega |(\nabla\times\mathbf{E})|^2 - k_0^2\boldsymbol{\epsilon_r}|\mathbf{E}|^2\,\mathrm{d}\Omega = jk_0Z_0\oint_{\partial\Omega}(\hat{\mathbf{n}}\times\mathbf{H})\cdot\overline{\mathbf{E}}\,\mathrm{ds}$$

where the right hand side surface integral can also be written as

$$\oint_{\partial\Omega}(\hat{\mathbf{n}}\times\mathbf{H})\cdot\overline{\mathbf{E}}\,\mathrm{ds} = -\oint_{\partial\Omega}(\hat{\mathbf{n}}\times\overline{\mathbf{E}})\cdot\mathbf{H}\,\mathrm{ds} = -\oint_{\partial\Omega}(\overline{\mathbf{E}}\times\mathbf{H})\cdot\hat{\mathbf{n}}\,\mathrm{ds}$$

so that to indicate the type of measurement available for the problem and thereafter that the total energy flux Ψ crossing the boundary of the domain is stored and dissipated within its interior, since

$$\Psi = \mathrm{Re}\oint_{\partial\Omega}\hat{\mathbf{n}}\cdot(\overline{\mathbf{E}}\times\mathbf{H})\,\mathrm{ds} = \mathrm{Re}\oint_{\partial\Omega}(\hat{\mathbf{n}}\times\overline{\mathbf{E}})\,\mathbf{H}\,\mathrm{ds} \tag{7.1.7}$$

where $\overline{\mathbf{E}}\times\mathbf{H}$ is the Poynting vector. Keeping the weak equation which includes the measurements we have for the problem we allow perturbations in each component of the permittivity tensor $\boldsymbol{\epsilon}\to\boldsymbol{\epsilon}+\delta\boldsymbol{\epsilon}$, and boundary data $\mathbf{E}\to\mathbf{E}+\delta\mathbf{E}$. Substituting into the above yields

$$\int_\Omega |(\nabla\times\mathbf{E})|^2 - k_0^2(\epsilon+\delta\epsilon)\mathbf{E}\,\overline{\mathbf{E}}\,\mathrm{d}\Omega = -jk_0Z_0\oint_{\partial\Omega}(\hat{\mathbf{n}}\times(\overline{\mathbf{E}}+\delta\overline{\mathbf{E}}))\,\mathbf{H}\,\mathrm{ds}$$

and simplifying by neglecting second and higher order terms in $\delta\epsilon$ and $\delta(\hat{\mathbf{n}}\times\mathbf{E})$ we get

$$\int_\Omega \delta\epsilon\,\mathbf{E}\,\overline{\mathbf{E}}\,\mathrm{d}\Omega = jk_0^{-1}Z_0\oint_{\partial\Omega}\delta(\overline{\hat{\mathbf{n}}\times\mathbf{E}})\,\mathbf{H}\,\mathrm{ds} \tag{7.1.8}$$

In the above note the distinction between $\delta\boldsymbol{\epsilon}\in\mathbf{X}$ the perturbation in the dielectric tensor, and $\delta\epsilon\in\mathbb{R}$ the perturbation along the i'th axes of the permittivity tensor, where $i\in\{xx,xy,xz,yy,yz,zz\}$. Recall that initially we have taken the test function to be equal to the electric field so that we get an estimate on the power dissipation in the system. When the permittivity is perturbed the electric field in the domain will change. We now focus our attention to the left hand side of (7.1.8) to quantify exactly the two electric fields involved. To simplify our notation we consider the k'th element in the model, the ψ^{ext} excitation and the m'th measurement with adjoint source $\mathbf{s}^m$. The relation

$$\left\langle M_{(\boldsymbol{\epsilon})}\begin{bmatrix}\delta\mathbf{E}(\psi^{ext})\\ \delta\mathbf{H}_s(\psi^{ext})\end{bmatrix},\begin{bmatrix}\mathbf{E}(\mathbf{s}^m)\\ \mathbf{H}_s(\mathbf{s}^m)\end{bmatrix}\right\rangle_{L_2} = \left\langle\begin{bmatrix}\delta\epsilon\,\mathbf{E}(\psi^{ext})\\ 0\end{bmatrix},\begin{bmatrix}\mathbf{E}(\mathbf{s}^m)\\ \mathbf{H}_s(\mathbf{s}^m)\end{bmatrix}\right\rangle_{L_2} \tag{7.1.9}$$

by virtue of (7.1.2), indicates that the perturbation in the total power within the domain can be recovered by one direct and one adjoint forward solutions. The right hand side of the above can be developed into

$$\left\langle\begin{bmatrix}\delta\epsilon\,\mathbf{E}(\psi^{ext})\\ 0\end{bmatrix},\begin{bmatrix}\mathbf{E}(\mathbf{s}^m)\\ \mathbf{H}_s(\mathbf{s}^m)\end{bmatrix}\right\rangle_{L_2} = \int_{\Omega_k}\delta\epsilon\,\mathbf{E}(\psi^{ext})\,\mathcal{E}(\mathbf{s}^m)\,\mathrm{d}\Omega \tag{7.1.10}$$

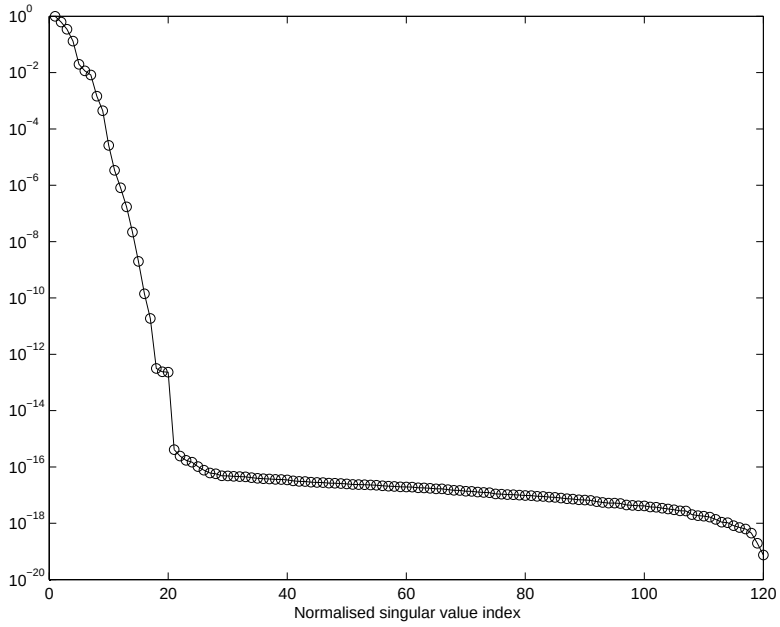

FIGURE 8. The normalized singular values of the Jacobian matrix revealing its ill-conditioning.

hence the element of the Jacobian matrix corresponding to the k'th element in the model, the ψ^{ext} experiment and the m'th measurement is given by

$$J^k_{(\psi^{ext},m)} = \frac{\delta(\hat{\mathbf{n}} \times \mathbf{E})}{\delta \boldsymbol{\epsilon}_{(i,w)}} = -jk_0 Y_0 \int_{\Omega_k} \mathbf{E}^i(\psi^{ext})\, \mathcal{E}^w(\mathbf{s}^m)\, \mathrm{d}\Omega \tag{7.1.11}$$

for $i, w \in \{x, y, z\}$. Relevant proofs for the Jacobian and its adjoint operator can be found in Somersalo et al. [36] and Dorn et al. [8]. The Fréchet derivative of the forward operator is linear, bounded and compact in the Hilbert spaces under consideration, and hence the Jacobian matrix is ill-conditioned. The degree of ill-posedness in the inverse problem is often assessed by examining the properties of the induced Jacobian in the linear formulation. A rather conventional tool for operator with exponentially decaying singular values. Computing the singular value decomposition of the Jacobian matrix reveals that these decay exponentially which is indicative of the severe form of ill-posedness in the problem. A plot of Jacobian's singular values for a typical configuration appears in figure 8. From this graph it becomes apparent that the matrix is badly scaled-conditioned with respect to inversion, and most importantly that the smallest singular values are well below the noise level in the system, making their filtration essential for preserving the stability in the reconstructed solution.

8. Inverse problem

For the inverse problem we assume the knowledge of a finite element model of the problem and an array of noise infused boundary measurements $\tilde{\zeta} \in \mathbf{Z}$ so that if $\zeta^* = \Phi(\boldsymbol{\epsilon}^*) \in \mathbf{Z}$ are the exact boundary data due to the target distribution then $\tilde{\zeta} = \zeta^* + \mathcal{N}(0, \sigma^2)$. Without any loss of generality we may further assume a Gaussian

noise signal of zero mean and standard deviation σ. For the construction of the inverse problem we first formulate the error norm residual function $f : \mathbf{X} \to \mathbf{R}$

$$f(\boldsymbol{\epsilon}) = \frac{1}{2}\big\|\zeta^* - \tilde{\zeta}\big\|_{\mathbf{Z}}^2 \tag{8.0.12}$$

which by substituting the forward operator yields the required inverse solution $\boldsymbol{\epsilon}^*$ by means of a nonlinear minimization problem

$$\boldsymbol{\epsilon}^* = \arg\min_{\epsilon\in\mathbf{X}} \frac{1}{2}\big\|\Phi(\boldsymbol{\epsilon}^*) - \tilde{\zeta}\big\|_{\mathbf{Z}}^2 \tag{8.0.13}$$

If $\boldsymbol{\epsilon}_0 \in \mathbf{X}$ is a strictly feasible initial guess on the dielectric tensor profile in a uniaxially anisotropic hybrid aligned (HAN) cell, so that $\boldsymbol{\epsilon}_0 \neq \boldsymbol{\epsilon}^*$ and the perturbation $\delta\boldsymbol{\epsilon} = \boldsymbol{\epsilon}^* - \boldsymbol{\epsilon}_0$ satisfies $\|\delta\boldsymbol{\epsilon}\|_{\mathbf{X}} \leq t$ for a small scalar t, then from a first-order Taylor expansion of f around ϵ_0 we obtain the linearized inverse problem as

$$\delta\boldsymbol{\epsilon}^* = \arg\min_{\delta\boldsymbol{\epsilon}\in\mathbf{X}} \frac{1}{2}\big\|\Phi'(\boldsymbol{\epsilon}_0)\delta\boldsymbol{\epsilon} - \delta\tilde{\zeta}\big\|_{\mathbf{Z}}^2 \tag{8.0.14}$$

where $\delta\tilde{\zeta} = \tilde{\zeta} - \Phi(\boldsymbol{\epsilon}^*)$. While for the generalized permittivity tensor imaging one would approach the problem (8.0.14), for the special case of the inverse director problem one has to formulate the optimization problem with respect to the distribution of directors $\mathbf{x}$. In this respect, we allow the following assumption.

Proposition 8.0.1. *In the special case of the uniaxial nematic liquid crystals, a perturbation in the boundary polarization measurements can be caused only by a perturbation in the directors. In effect, $\delta\boldsymbol{\epsilon}$ implies $\delta\mathbf{x}$, and if the operator $\Phi_{\mathbf{x}} : \mathbb{L}^2(\Omega)^3 \to \mathbf{Z}$ maps distributions of directors in the interior of the domain to their corresponding boundary data*

$$\Phi_{\mathbf{x}} \triangleq \mathbf{x}\big|_{\Omega} \to \hat{\mathbf{n}} \times \mathbf{E}\big|_{\Gamma_1} \tag{8.0.15}$$

then

$$\Phi'(\boldsymbol{\epsilon}) = \Phi'_{\mathbf{x}}(\mathbf{x}) \tag{8.0.16}$$

for all $\boldsymbol{\epsilon}$, $\mathbf{x}$ satisfying (1.1.2).

As before $\mathbf{x}^* \in \mathbb{L}^2(\Omega)^3$ is the target solution we seek to reconstruct, and for which we possess an array of noisy measurements $\tilde{\zeta}$. In this setting the inverse problem is expressed as

$$\min_{\mathbf{x}\in\mathbb{L}^2(\Omega)^3} \frac{1}{2}\big\|\Phi_{\mathbf{x}}(\mathbf{x}^*) - \tilde{\zeta}\big\|_{\mathbf{Z}}^2 \tag{8.0.17}$$

Repeating the linearization procedure for the new objective at the point $\mathbf{x}_0$ satisfying $\boldsymbol{\epsilon}_0 = \mathbf{x}_0 \otimes \mathbf{x}_0 + I$, and computing the Fréchet derivative of $\Phi_{\mathbf{x}}$ at $\mathbf{x}_0$ we can formulate a linearized inverse problem for estimating the optimum value of the perturbation $\delta\mathbf{x}^* = \mathbf{x}^* - \mathbf{x}_0$ as

$$\delta\mathbf{x}^* = \arg\min_{\delta\mathbf{x}\in\mathbb{L}^2(\Omega)^3} \frac{1}{2}\big\|\Phi'_{\mathbf{x}}(\mathbf{x}_0)\delta\mathbf{x} - \delta\tilde{\zeta}\big\|_{\mathbf{Z}}^2 \tag{8.0.18}$$

where $\delta\tilde{\zeta} = \tilde{\zeta} - \Phi_{\mathbf{x}}(\mathbf{x}^*)$. For the formulation of the problem (8.0.18) it suffices to compute the Jacobian $\Phi'_{\mathbf{x}}(\mathbf{x}_0)$ with respect to the directors. Writing the weak form of the forward problem with respect to the directors we have

$$\int_{\Omega} |(\nabla\times\mathbf{E})|^2 - k_0^2(\mathbf{x}\otimes\mathbf{x} + I)\mathbf{E}\,\overline{\mathbf{E}}\,\mathrm{d}\Omega = -jk_0Z_0 \oint_S (\overline{\hat{\mathbf{n}}\times\mathbf{E}})\mathbf{H}\,\mathrm{ds} \tag{8.0.19}$$

Taking perturbations on the measurements and each vector component of the director $\mathbf{x}_i \to \mathbf{x}_i + \delta\mathbf{x}_i$ for $i \in \{x, y, z\}$, and simplifying we arrive at

$$-k_0^2 \int_\Omega \mathbf{E}(2\mathbf{x}_i\delta\mathbf{x}_i + \delta\mathbf{x}_i\delta\mathbf{x}_i)\mathbf{F}\,\mathrm{d}\Omega = -jk_0Z_0 \oint_S \delta(\overline{\hat{\mathbf{n}} \times \mathbf{E}})\mathbf{H}\,\mathrm{ds} \tag{8.0.20}$$

Neglecting second order term $\delta\mathbf{x}_i\delta\mathbf{x}_i$ and rearranging yields an expression for the k'th element of the discrete Jacobian matrix as

$$J^k_{(\mathbf{x}_{0,i},\psi^{ext},m)} = \frac{\delta(\hat{\mathbf{n}} \times \mathbf{E})}{\delta\mathbf{x}_i} = -2jk_0Y_0 \int_{\Omega_k} \mathbf{x}_{0,i}\,\mathbf{E}^i(\psi^{ext})\,\mathcal{E}^i(\mathbf{s}^m)\,\mathrm{d}\Omega \tag{8.0.21}$$

for $i = x, y, z$. With the computed Jacobian the linearized inverse problem (8.0.18) becomes

$$\delta\mathbf{x}^* = \arg\min_{\delta\mathbf{x}\in\mathbb{L}^2(\Omega)^3} \frac{1}{2}\big\|J_{(\mathbf{x}_0,\psi^{ext},m)}\delta\mathbf{x} - \delta\tilde{\zeta}\big\|^2_{\mathbf{Z}} \tag{8.0.22}$$

where $J_{(\mathbf{x}_0,\psi^{ext},m)} \in \mathbb{C}^{3m\times 3k}$, $\delta\mathbf{x} \in \mathbb{R}^{3k}$ and $\delta\tilde{\zeta} \in \mathbb{C}^{3m}$. As the problem is ill-posed, we augment the program (8.0.22) with a regularizing prior information inequality constraint $C(\mathbf{x}) \le t$, where $C : \mathbf{X} \to \mathbb{R}$ is derived from Frank's energy formula like

$$C(\mathbf{x}) = \frac{1}{2}K_{11}\big(\nabla\cdot\mathbf{x}\big)^2 + \frac{1}{2}K_{22}\big(\mathbf{x}\cdot(\nabla\times\mathbf{x})\big)^2 + \frac{1}{2}K_{33}\big(\mathbf{x}\times(\nabla\times\mathbf{x})\big)^2 \tag{8.0.23}$$

for $t \in \mathbb{R}$ is a small constant. Under the assumption that the three elastic constants are of the same magnitude we adopt the one constant approximation of C [11], where the elastic constants are taken to be the same, e.g. $K_{11} = K_{22} = K_{33} = K$. In this case the energy constraint simplifies to a Dirichlet integral term

$$C(\mathbf{x}) \simeq K|\nabla\mathbf{x}|^2 = K\sum_{i=x,y,z}(\partial_i\mathbf{x})^2 \tag{8.0.24}$$

which is known to minimize C locally in stable and quasi-stable configurations of $\mathbf{x}$ [22]. Alternative regularization priors for nematic cells can be derived from Landau–de Gennes free energy [24], which is based on temperature, volume, the local tensor order and its spatial derivatives. For the regularized problem, we seek a perturbation in the director that satisfies

$$\delta\mathbf{x}^* = \arg\min_{\delta\mathbf{x}} \frac{1}{2}\Big\|J\,\delta\mathbf{x} - \delta\zeta\Big\|_2^2 \quad \text{such that} \quad \big\{\|D^x\delta\mathbf{x}\|_2^2 + \|D^y\delta\mathbf{x}\|_2^2 + \|D^z\delta\mathbf{x}\|_2^2\big\} \le t \tag{8.0.25}$$

where $D^x = \partial_x \in \mathbb{R}^{3k\times 3k}$, $D^y = \partial_y \in \mathbb{R}^{3k\times 3k}$ and $D^z = \partial_z \in \mathbb{R}^{3k\times 3k}$ are positive definite gradient matrix operators as in (8.0.24). In this context the generalized Tikhonov solution of (8.0.25) is

$$\delta\mathbf{x} = \Big(J^*J + \kappa^2\big((D^x)^*(D^x) + (D^y)^*(D^y) + (D^z)^*(D^z)\big)\Big)^{-1}\,J^*\delta\zeta \tag{8.0.26}$$

for a regularization parameter $\kappa > 0$.

9. Numerical results

Consider a closed domain $\Omega \in [0,1]\times[0,1]\times[0,1]$ with a piecewise constant director profile

$$\mathbf{x}_i^* = \begin{cases} \Big[\cos(2z_i)\cos(2x_i) \quad \cos(2z_i)\sin(2x_i) \quad \sin(2z_i)\Big] & \text{at element } i, \\ 0 & \text{otherwise.} \end{cases}$$

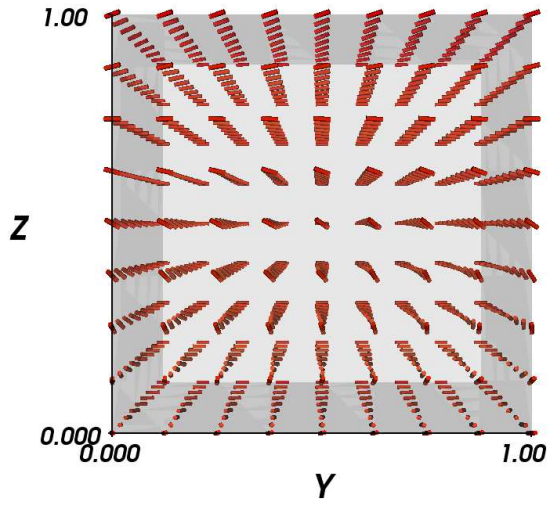

(a) Side view of $\mathbf{x}^*$.

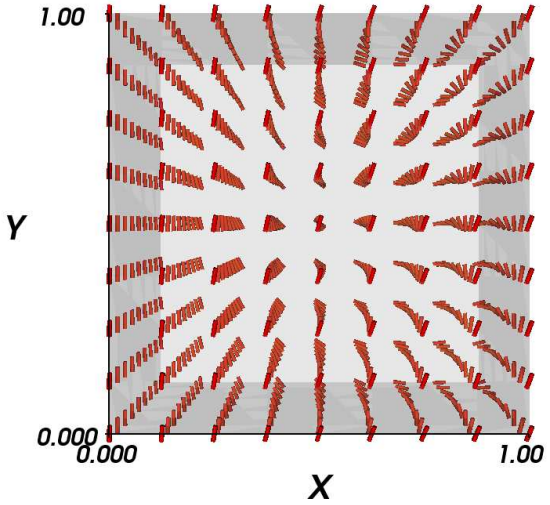

(b) Top view of $\mathbf{x}^*$.

FIGURE 9. The target distribution of director vectors in a HAN uniaxial liquid crystal cell.

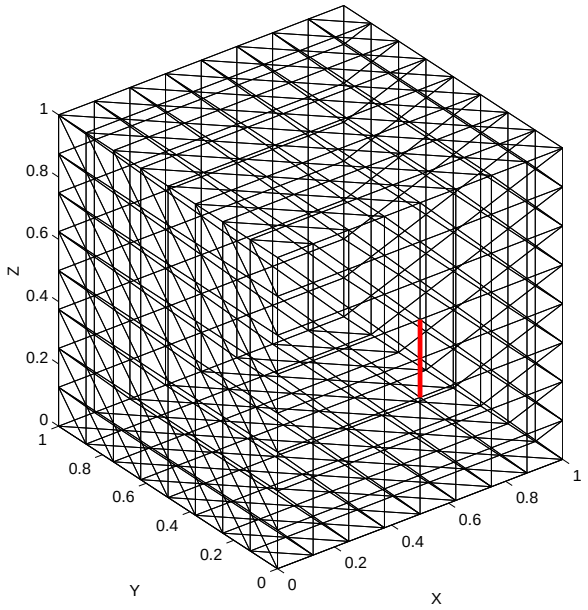

FIGURE 10. The point at which the incident radiation enters the liquid crystal cell.

where (x_i, y_i, z_i) denotes the center of the i'th element in the model. The distribution of directors in consideration is shown in figure 9. The wavelength of the incoming radiation was taken to be five times the mean length of the edges in the model, resulting in wave propagation constant of $k_0 = 2.0521$. The incident polarization angles were taken at $\theta = \pi/2$ and $\phi = 0$, yielding an incident polarization vector $\hat{\mathbf{p}}^i = \begin{bmatrix} 1 & 1 & 0 \end{bmatrix}$. Figure 10 shows the part of the boundary where the incoming radiation enters the liquid crystal. Based on the model $\mathbf{x}^*$, an array of 27 measurements ζ^*, have been simulated at detector positions located on horizontal boundary edges throughout the periphery of the model. To the exact data we have subsequently added a Gaussian noise signal of zero mean and standard deviation $\sigma = 0.001 \cdot \|\mathrm{Re}(\zeta^*)\|$, yielding $\tilde{\zeta}$, so that to incorporate the effect of physical noise and instrumentation precision.

Taking an initial guess on the solution $\mathbf{x}_0 \in \mathbf{X}$, so that $\|\mathbf{x}^* - \mathbf{x}_0\|_{\mathbf{X}}$ is small, for nonzero displacements in the Euler angles of the director $\delta\theta = 0.06$ and $\delta\phi = 0.04$ radians, we have

$$\mathbf{x}_0^* = \begin{cases} \begin{bmatrix} \cos(2z_i + \delta\theta)\cos(2x_i + \delta\phi) \\ \cos(2z_i + \delta\theta)\sin(2x_i + \delta\phi) \\ \sin(2z_i + \delta\theta) \end{bmatrix} & \text{at element } i, \\ 0 & \text{otherwise.} \end{cases}$$

For the initial guess we compute the forward solution $\Phi(\mathbf{x}_0)$, $\delta\tilde{\zeta} = \zeta^* - \Phi(\mathbf{x}_0)$ and thereafter evaluate the Jacobian matrix at $\mathbf{x}_0$ using equation (8.0.21). Assembling the gradient operators using [29], we set up the linearized problem (8.0.22), and

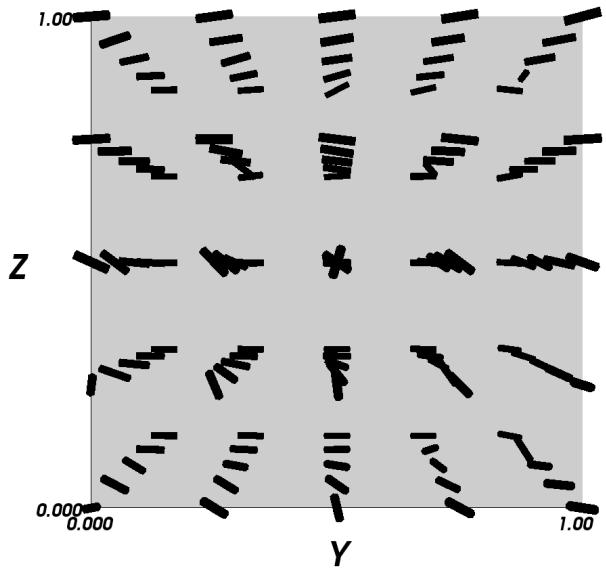

(a) Side view of reconstructed $\mathbf{x}$.

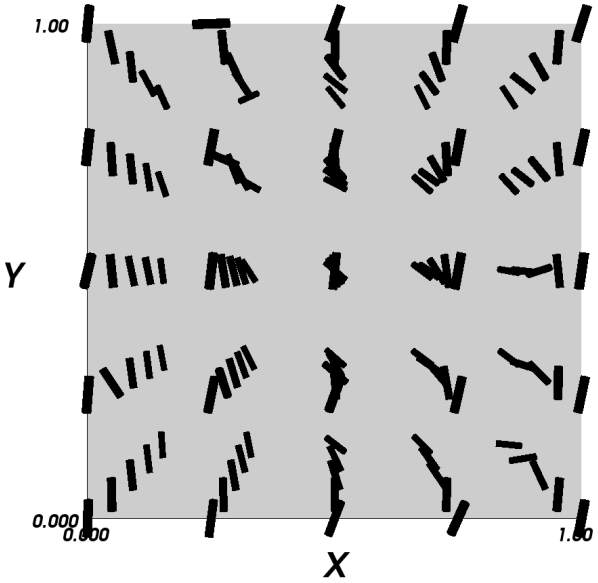

(b) Top view of reconstructed $\mathbf{x}$.

FIGURE 11. The reconstructed distribution of director vectors in a HAN uniaxial liquid crystal cell.

setting the regularization parameter $k = 2\sigma$, we compute the Tikhonov solution using (8.0.26). Images of the reconstructed solution appear in figure 11. The images illustrate a close resemblance between the original-target and reconstructed director distributions but at the same time are indicative of the impact of noise to the problem, causing some local discontinuities in the otherwise smooth orientation profile. The algorithm can easily be extended for nonlinear reconstruction by feeding the Tikhonov linear step solver within the Newton's iterative scheme as in [28].

10. Conclusions

In this report we have derived the forward problem for high-frequency wave propagation in nematic liquid crystals. We have developed a numerical model based on a hybridization of vector finite elements with a boundary integral equation imposing the Neumann boundary conditions. This formulation yields surface integrals with singular kernels in the combinations of nearby located elements which we treat numerically using a special basis of surface functions, numerical integration and closed form expressions. In the resulted forward problem we solve for the electric field in the closure of the domain as well as the tangential of the magnetic field at the boundary, thus the problem leads conveniently to the formulation of the linearized inverse problem via the computation of the Jacobian of the forward mapping via the method of the adjoint fields. The inverse director orientation problem in the uniaxial nematic crystal cell, we approached as a special case of the anisotropic permittivity tensor imaging problem, aiming to recover the two distinctive eigenvalues of the permittivity tensor. For the linearized inverse problem we adopt a generalized Tikhonov regularization approach, using a prior information functional derived from Frank's energy minimization formula that holds in stable nematic configurations. The numerical results indicate that the director orientation profile can be reconstructed from an adequate set of boundary polarization measurements gathered perimetrically.

Acknowledgments

The author is grateful to the Smith Institute for the Faraday Partnership, EPSRC for the grant GR/R93612/01 and Hewlett Packard Laboratories Bristol for their support. In particular I would like to thank Bill Lionheart at the School of Mathematics at the University of Manchester, and Chris Newton at Hewlett Packard Research Labs Bristol for introducing me into the interesting world of liquid crystal optics, as well as Nigel Mottram at the School of Mathematics at the Strathclyde University and Melvin Brown at the Smith Institute for their guidance and support.

References

[1] M. Becchi and P. Galatola, *Berreman-matrix formulation of light propagation in stratified anisotropic chiral media*, European Physical Journal B, vol. 8, pp. 399-404.

[2] D.W. Berreman, *Optics in stratified and anisotropic media: 4×4 matrix formulation*, Journal of the Optical Society of America, vol. 62, no. 4, 1971.

[3] A. Bossavit, *Computational electromagnetism: Variational formulations, complementarity, edge elements*, CA Academic press, San Diego, 1998.

[4] A. Bossavit, *Mixed finite elements and the complex of Whitney forms*, in 'The Mathematics of finite elements and applications VI', CA Academic press, San Diego, 1988.

[5] S. Chandrasekhar, *Liquid Crystals*, Cambridge University press, New York, 1992.
[6] A. Chatterjee, J.M. Jin and J.L. Volakis, *Edge-based finite elements and vector ABC's applied to 3D scattering*, IEEE transactions on antennas and propagation, vol. 41, no. 2, 1993.
[7] M.D. Deshpande, C.J. Reddy, P.I. Tiemsin and R. Cravey, *A new approach to estimate complex permittivity of dielectric materials at microwave frequencies using waveguide measurements*, IEEE transactions on microwave theory and techniques, vol. 45, no. 3, pp. 359-366, 1997.
[8] O. Dorn, H. Bertete-Aquirre, J.G. Berryman and G.C. Papanicolaou, *Sensitivity analysis of a nonlinear inversion method for 3D electromagnetic imaging in anisotropic media*, Inverse problems, vol. 18, pp. 285-317, 2002.
[9] T.F. Eibert and V. Hansen, *On the calculation of potential integrals for linear source distributions on triangular domains*, IEEE transactions on antennas and propagation, vol. 43, no. 12, pp. 1499-1502, 1995.
[10] P. Galatola and C. Oldano, *Theory of linear optics of liquid crystals*, In 'The Optics of Thermotropic Liquid Crystals' edited by S.J. Elston and J. R. Sambles, Taylor & Francis, London, 1992.
[11] P.G. de Gennes and J. Prost, *The Physics of Liquid Crystals*, 2nd ed., Oxford University press, New York, 1993.
[12] C. Geuzaine, B. Meys, F. Henrotte, P. Dular and W. Lergos, *A Galerkin method for mixed finite elements*, IEEE transactions on magnetics, vol. 35, no. 3, 1999.
[13] J. Gong, J.L. Volakis, A.C. Woo and H.T.G. Wang, *A hybrid finite element-boundary integral method for the analysis of cavity-backed antennas of arbitrary shape*,IEEE transactions on antennas and propagation, vol. 42, no. 9, pp. 1233-1242, 1994.
[14] R.D. Graglia, *On the numerical integration of the linear shape functions times the 3D Green's function or its gradient on a plane triangle*, IEEE transactions on antennas and propagation, vol. 41, no. 10, pp. 1448-1455, 1993.
[15] E. Haber and U.M. Ascher, *Fast finite volume simulation of 3D electromagnetic problems with highly discontinuous coefficients*, SIAM Journal of Scientific Computing, vol. 22, no. 6, pp. 1943-1961.
[16] R.E. Hodges and Y. Rahmat-Samii, *The evaluation of MFIE integrals with the use of vector triangle basis functions*, Microwave and optical technology letters, vol. 14, pp. 9-14, 1997.
[17] J.M. Jin, *The finite element method in electromagnetics*, 2nd ed., John Wiley & Sons, New York, 2002.
[18] J.M. Jin and J.L. Volakis, *Electromagnetic scattering by and transmission through a three-dimensional slot in a thick conducting plane*, IEEE transactions on antennas and propagation, vol. 39, no. 4, 1991.
[19] J.M. Jin, J.L. Volakis and J.F. Collins *A finite element-boundary integral method for scattering and radiation by two and three dimensional structures*, IEEE antennas and propagation magazine, vol. 39, no. 3, 1991.
[20] E.E. Kriezis, Newton C.J., Spiller T.P. and Elston S. J., *3D Simulations of Light Propagation in periodic Liquid Crystal Microstructures*, Applied Optics, vol. 41, no. 25, pp. 5346-5356, 2002.
[21] M. Lassas, M. Cheney and G. Uhlmann, *Uniqueness for a wave propagation inverse problem in a half-space*, Inverse Problems, vol. 4, pp. 679-684, 1998.
[22] A. Majumdar, J.M. Robbins and M. Zyskin, *Elastic energy of liquid crystals in convex polyhedra*, Journal of Physics A: Mathematical and General, vol. 37, pp. L573-L580, 2004.
[23] MATLAB: The language of technical computing, Mathworks Inc. http://www.mathworks.com, 2004.
[24] N. Mottram and C.J.P. Newton, *Introduction to Q-tensor theory*, Technical Report, Department of Mathematics, University of Strathclyde, UK, 2004.
[25] C.J.P. Newton and T.P. Spiller, *A novel approach to modelling nematic liquid crystal cells*, HPL-2000-109 technical report, HP labs, Bristol, UK.
[26] P.Y. Oijala and M. Taskinen, *Calculation of CFIE impedance matrix elements with RWG and $n \times$ RWG functions*, IEEE transactions on antennas and propagation, vol. 51, no. 8, 2003.
[27] K.D. Paulsen, D.R. Lynch and J.W. Strohbehn, *Three-dimensional finite, boundary, and hybrid element solutions of the Maxwell equations for lossy dielectric media*, IEEE transactions on microwave theory and techniques, vol. 36, no. 4, pp. 682-693, 1988.

[28] N. Polydorides, *Image reconstruction algorithms for soft-field tomography*, Ph.D. thesis, University of Manchester (UMIST), 2002.
[29] N. Polydorides and W.R.B. Lionheart, *A Matlab toolkit for three dimensional Electrical Impedance Tomography: A contribution to the EIDORS project*, Measurement Science and Technology, vol. 13, no. 12, pp. 1871-1883, 2002.
[30] R.W. Ruhwandl and E.M. Terentjev, *Monte Carlo simulation of topological defects in the nematic liquid crystal matrix around a spherical colloid particle*, Physical Review E, vol. 56, no. 5, pp. 5561-5565, 1997.
[31] C.J. Reddy, M.D. Deshpande, C.R. Cockrell and F.B. Beck, *Electromagnetic scattering analysis of a three-dimensional cavity-backed aperture in an infinite ground plane using a combined finite element method/method of moments approach*, NASA technical paper 3544, Langley research center, 1995.
[32] C.J. Reddy, M.D. Deshpande, C.R. Cockrell and F.B. Beck, *Finite element method for eigenvalue problems in electromagnetics*, NASA technical paper 3485, Langley research center, 1994.
[33] X.Q. Sheng, J.M. Jin, J. Song, W.C. Chew and C.C. Lu, *Solution of combined field integral equation using multilevel fast multiple algorithm for scattering by homogeneous bodies*, IEEE transactions on antennas and propagation, vol. 46, no. 11, 1998.
[34] P.P. Silverster and R.L. Ferrari, *Finite elements for Electrical engineers*, 3rd ed., Cambridge University press, New York, 1996.
[35] N.M. Silvestre, P. Patricio, M. Tasinkevych, D. Andrienko and M.M. Telo da Gama, *Colloidal discs in nematic liquid crystals*, Journal of Physics of Condensed Matter, vol. 16, pp. S1921-S1930, 2004.
[36] E. Somersalo, D. Isaacson and M. Cheney, *A linearized inverse boundary value problem for Maxwell's equations*, Journal of Computational & Applied Mathematics, vol. 42, pp. 123-136, 1992.
[37] C.T. Tai, *Dyadic Green's functions in electromagnetic theory*, 2nd ed., IEEE press, New York, 1994.
[38] A. Tzoulis and T.F. Eibert, *Review of singular potential integrals for method of moments solutions of surface integral equations*, Advances in Radio Science, vol. 2, pp. 93-99, 2004.
[39] J.L. Volakis, A. Chatterjee and L.C. Cempel, *Finite element method for electromagnetics: Antennas, microwave circuits, and scattering applications*, IEEE press, New York, 1998.
[40] D.R. Wilton, S.M. Rao, A.W. Glisson, D.H. Schaubert, O.M. Al-Bundak and C.M. Butler, *Potential integrals for uniform and linear source distributions on polygonal and polyhedral domains*, IEEE Transactions of antennas and propagation, vol. AP-31, pp 276-281, 1984.
[41] H. Wöhler and M.E. Becker, *Numerical modelling of LCD electro-optical performance*, Optoelectronics Review, vol. 10, no. 1, pp 23-33, 2002.
[42] X. Yuan, D. R. Lynch and J.W. Strohbehn, *Coupling of finite element and moment methods for electromagnetic scattering from inhomogeneous objects*, IEEE transactions on antennas and propagation, vol. 38, no. 3, 1990.

Inverse Problems Group, School of Mathematics, University of Manchester, PO Box 88, Manchester, M60 1QD, UK.
E-mail address: nick.polydorides@manchester.ac.uk